



---

MSU Graduate Theses

---

Spring 2019

## Synthesis, Stabilization, and Modification of Zinc Oxide Nanoparticles for Biological Applications


Allison Kimberly Freese

Missouri State University, Freese621@live.missouristate.edu

As with any intellectual project, the content and views expressed in this thesis may be considered objectionable by some readers. However, this student-scholar's work has been judged to have academic value by the student's thesis committee members trained in the discipline. The content and views expressed in this thesis are those of the student-scholar and are not endorsed by Missouri State University, its Graduate College, or its employees.

---

Follow this and additional works at: <https://bearworks.missouristate.edu/theses>

 Part of the [Analytical Chemistry Commons](#), [Biochemistry Commons](#), and the [Inorganic Chemistry Commons](#)

### Recommended Citation

Freese, Allison Kimberly, "Synthesis, Stabilization, and Modification of Zinc Oxide Nanoparticles for Biological Applications" (2019). *MSU Graduate Theses*. 3370.  
<https://bearworks.missouristate.edu/theses/3370>

This article or document was made available through BearWorks, the institutional repository of Missouri State University. The work contained in it may be protected by copyright and require permission of the copyright holder for reuse or redistribution.

For more information, please contact [bearworks@missouristate.edu](mailto:bearworks@missouristate.edu).

**SYNTHESIS, STABILIZATION, AND MODIFICATION OF ZINC OXIDE  
NANOPARTICLES FOR BIOLOGICAL APPLICATIONS**

A Master's Thesis

Presented to

The Graduate College of  
Missouri State University

In Partial Fulfillment

Of the Requirements for the Degree  
Master of Science, Chemistry

By

Allison Kimberly Freese

May 2019

Copyright 2019 by Allison Kimberly Freese

# **SYNTHESIS, STABILIZATION, AND MODIFICATION OF ZINC OXIDE NANOPARTICLES FOR BIOLOGICAL APPLICATIONS**

Chemistry

Missouri State University, May 2019

Master of Science

Allison Freese

## **ABSTRACT**

Nanoparticles have become very useful as delivery systems in biomedicine. The nanoparticles can be layered with different compounds to produce a vessel for transport of biological materials. Specifically, gold nanoparticles layered with a reducing agent, lysozyme, and polyelectrolytes can be synthesized to transport lysozyme into a cell. However, zinc oxide nanoparticles are cheaper, biocompatible nanoparticles that can be used for the same process. Here in, zinc oxide nanoparticle conjugates were synthesized, modified, and analyzed to be used as a biological material delivery system. The zinc oxide nanoparticles were synthesized using zinc chloride and sodium hydroxide. The particles were then layered using the layer-by-layer technique of adding each compound to the nanoparticle solution dropwise. Each deposition was bound by the interaction of the opposite charges of the compounds being added. The layers used were mercaptoundecanoic acid (MUA), poly(ethylenimine) (PEI), polystyrene sulfonate (PSS), and RNA or lysozyme ordered specifically to have a high affinity for binding each layer. With each deposition added to the system, the following instruments were used to characterize the particles: Dynamic Light Scattering Spectroscopy (DLS) and Scanning Electrons Microscopy (SEM) for particle sizing, Electrophoretic Mobility (ELS) for zeta potential and surface charge, and UV-Vis spectrophotometer and FTIR spectroscopy for optical properties. Furthermore, after the layering process was completed, the biological material encapsulated was tested to assure its effectiveness once transported into the cell. This was completed using an enzymatic assay for lysozyme and an ethidium bromide assay for RNA. After characterization was completed, all three nanoparticle conjugates were concluded to be successfully synthesized.

**KEYWORDS:** zinc oxide, protein, protein delivery, lysozyme, RNA, nanoparticles, nanomaterials, layer-by-layer.

**SYNTHESIS, STABILIZATION, AND MODIFICATION OF ZINC OXIDE  
NANOPARTICLES FOR BIOLOGICAL APPLICATIONS**

By

Allison Freese

A Master's Thesis  
Submitted to the Graduate College  
Of Missouri State University  
In Partial Fulfillment of the Requirements  
For the Degree of Master of Science, Chemistry

May 2019

Approved:

Adam K. Wanekaya, Ph.D., Thesis Committee Chair

Gary Meints, Ph.D., Committee Member

Erich Steinle, Ph.D., Committee Member

Kartik Ghosh, Ph.D., Committee Member

Julie Masterson, Ph.D, Dean of the Graduate College

In the interest of academic freedom and the principle of free speech, approval of this thesis indicates the format is acceptable and meets the academic criteria for the discipline as determined by the faculty that constitute the thesis committee. The content and views expressed in this thesis are those of the student-scholar and are not endorsed by Missouri State University, its Graduate College, or its employees.

## ACKNOWLEDGEMENTS

I dedicate this thesis to my friends and family who helped me through my entire college experience. Without their love and support, my success would not have been possible. There were times I didn't think I would make it through, but my family never stopped believing in me. Specifically, I would like to thank my parents, Mike and Julee Freese, my boyfriend, Jacob Trammell, and my siblings, Kevin and Matthew Freese. This would not have been possible without each and every one of you.

I would also like to thank my advisor, Dr. Adam Wanekaya, for having me in his lab all these years and helping me to become the chemist that I am. Furthermore, I'd like to thank Dr. Gary Meints, Dr. Kayte Fichter, and Dr. Gautam Bhattacharyya for their help and support throughout college. Lastly, I'd like to thank all my fellow students and research members who helped with the project and kept me sane through all of it, especially Megan Prado, Molly Duszynski, and Arkanil Roy.

## TABLE OF CONTENTS

Chapter 1. Introduction .....	1
Section 1.1 Nanoparticles as a Delivery Platform .....	1
Section 1.2 Past Research with Gold Nanoparticles .....	7
Section 1.3 Zinc Oxide Nanoparticles .....	17
Section 1.4 Motivations .....	22
Section 1.5 Objectives .....	23
Chapter 2. Experimental .....	24
Section 2.1 Materials .....	24
Section 2.2 Methods.....	24
Section 2.2.1 Dynamic Light Scattering Spectroscopy .....	25
Section 2.2.2 Electrophoretic Mobility Light Scattering Spectroscopy .....	26
Section 2.3 Synthesis of PEI-PSS-Lys-MUA-ZnO NPs .....	29
Section 2.4 Synthesis of PEI-PSS-Lys-ZnO NPs .....	31
Section 2.5 Lysozyme Activity Assay .....	32
Section 2.6 Synthesis of PEI-RNA-PEI-MUA-ZnO NPs.....	33
Section 2.7 RNA Integrity Analysis .....	35
Chapter 3. Results and Discussion.....	37
Section 3.1 Encapsulation of Lysozyme.....	38
Section 3.1.1 UV-Vis Spectrophotometry.....	38
Section 3.1.2 Scanning Electron Microscopy .....	41
Section 3.1.3 Dynamic Light Scattering .....	43
Section 3.1.4 Zeta Potential.....	47
Section 3.1.5 Fourier-Transform Infrared Spectroscopy.....	50
Section 3.1.6 Activity of Lysozyme .....	53
Section 3.2 Encapsulation of RNA .....	55
Section 3.2.1 UV-Vis Spectrophotometry.....	55
Section 3.2.2 Scanning Electron Microscopy .....	56
Section 3.2.3 Dynamic Light Scattering .....	57
Section 3.2.4 Zeta Potential.....	58
Section 3.2.5 Fourier-Transform Infrared Spectroscopy.....	59
Section 3.2.6 Integrity of RNA .....	60
Chapter 4. Conclusion.....	66
References.....	69

## ABBREVIATIONS

- AuNP:** Gold Nanoparticle  
**DLS:** Dynamic Light Scattering  
**DNA:** Deoxyribose Nucleic Acid  
**EB:** Ethidium Bromide  
**ELS:** Electrophoretic Mobility Light Scattering  
**FTIR:** Fourier-Transform Infrared Spectroscopy  
**HCl:** Hydrochloric Acid  
**IR:** Infrared Spectroscopy  
**KCl:** Potassium Chloride  
**Lys:** Lysozyme  
**MUA:** 11-Mercaptoundecanoic Acid  
**NaCl:** Sodium Chloride  
**NaOH:** Sodium Hydroxide  
**NP:** Nanoparticle  
**PBS:** Phosphate-Buffered Saline  
**PEI:** Polyethyleneimine  
**PSS:** Polystyrene(sulfonate)  
**RNA:** Ribonucleic Acid  
**SEM:** Scanning Electron Microscopy  
**UV-Vis:** Ultra Violet—Visible Light Spectrophotometry  
**XRD:** X-Ray Diffraction  
**ZnCl<sub>2</sub>:** Zinc Chloride  
**ZnO:** Zinc Oxide



## LIST OF TABLES

Table 1. Zeta potential values for MUA, PEI, PSS, Lysozyme, and RNA.....	48
--------------------------------------------------------------------------	----

## LIST OF FIGURES

Figure 1. Transporting a protein into a cell.....	4
Figure 2. Order of layers for the encapsulation of DNA .....	6
Figure 3. Methods for synthesizing AuNPs with layering.....	9
Figure 4. Enzymatic activities of free lysozyme and AuNP bioconjugates.....	11
Figure 5. The tertiary structure of lysozyme.....	12
Figure 6. Polyelectrolyte branched structures of PSS and PEI.....	13
Figure 7. Examples of Coalescence and Ostwald Ripening .....	14
Figure 8. General structure of Ribonucleic Acid .....	16
Figure 9. Common Zinc Oxide Crystal Structures .....	18
Figure 10. Reaction of the synthesis of zinc oxide nanoparticles.....	20
Figure 11. Binding mechanisms of gold and zinc to MUA .....	21
Figure 12. General Scheme of DLS Instrument.....	26
Figure 13. General Scheme of ELS Instrument .....	27
Figure 14. Coffee Mate Standard for ELS .....	28
Figure 15. Methods for synthesizing ZnO NPs with layering .....	30
Figure 16. Encapsulation of RNA Method for synthesizing ZnO NPs.....	34
Figure 17. XRD pattern for synthesized zinc oxide nanoparticles .....	37
Figure 18. Absorbance spectra for ZnO-MUA-Lys-PSS-PEI sample .....	39
Figure 19. Absorbance spectra for ZnO-Lys-PSS-PEI sample.....	40
Figure 20. SEM images before and after deposition for ZnO-Lys-PSS-PEI.....	41
Figure 21. SEM images before and after deposition for ZnO-MUA-Lys-PSS-PEI .....	42
Figure 22. Nanoparticle diameter versus reaction time for ZnO-MUA.....	44
Figure 23. Particle diameter and polydispersity of ZnO-MUA-Lys-PSS-PEI sample .....	45
Figure 24. Particle diameter and polydispersity of ZnO-Lys-PSS-PEI sample.....	46
Figure 25. Zeta potential of ZnO-MUA-Lys-PSS-PEI sample.....	48
Figure 26. Zeta potential of ZnO-Lys-PSS-PEI sample .....	49
Figure 27. FTIR Spectra for ZnO-Lys-PSS-PEI samples.....	51
Figure 28. FTIR Spectra for ZnO-MUA-Lys-PSS-PEI samples .....	52
Figure 29. Lysozyme activity assay.....	54
Figure 30. Absorbance Spectra for ZnO-MUA-PEI-RNA-PEI layered sample.....	55
Figure 31. SEM images before and after deposition for ZnO-MUA-PEI-RNA-PEI .....	57
Figure 32. Particle diameter and polydispersity of ZnO-MUA-PEI-RNA-PEI.....	58
Figure 33. Zeta potential of ZnO-MUA-PEI-RNA-PEI sample .....	59
Figure 34. FTIR Spectra for ZnO-MUA-PEI-RNA-PEI samples .....	60
Figure 35. Standard RNA integrity assay using acid for degradation .....	61
Figure 36. Standard RNA integrity assay using heat for degradation .....	62
Figure 37. RNA integrity assay for nanoparticle samples using acid for degradation .....	63
Figure 38. RNA integrity assay for nanoparticle samples using heat for degradation .....	64

## CHAPTER 1. INTRODUCTION

### Section 1.1 Nanoparticles as a Delivery Platform

The nanoscale has been researched immensely for over the last century beginning with Michael Faraday discovering that colloidal gold has a ruby red color.<sup>1</sup> Elemental gold is well known for the bright yellow, or gold, color that it has. However, on the nanoscale, it actually appears red or purple. From that point on, nanoscale materials were slowly making an appearance in the scientific field. Nanotechnology was first introduced by Richard P. Feynman in his 1959 lecture called “There’s Plenty of Room at the Bottom”.<sup>2</sup> He discussed the ground breaking idea of manipulating individual atoms. However, his lecture went unnoticed by the science world until the early 1980s. In 1985, Louis Brus made the discovery of colloidal semiconductor nanocrystals, termed quantum dots.<sup>1</sup> From there, in 1991, Sumino Lijima documented the first observation of carbon nanotubes. As nanomaterials and various instruments to analyze atoms and nanoscale materials continued to be investigated, nanotechnology companies began to emerge in the 1990s, such as Nanophase Technologies, Helix Energy Solutions Group, and Nano-Tex.<sup>1</sup> The science industry was fully embracing the discoveries of nanomaterials and nanotechnology, but the general public did not until the early 2000s when consumer products began using nanotechnology in their industries.<sup>1</sup> The entire world is now involved in nanomaterials and their development for products, science, medicine, etc.

The word “nanomaterial” is defined as a material with particles or constituents with dimensions measuring in the nanoscale, or something that is produced by nanotechnology.<sup>3</sup> Nanomaterials come in different types, morphologies, and dimensions. There are nanorods, nanoparticles, nanospheres, nanowires, quantum dots, etc. The main characteristic they all have

in common is that they are on the nanoscale in some way, where 1 nanometer (nm) equals  $10^{-9}$  meters. For example, a nanometer is approximately 100,000 times thinner than the diameter of a single human hair.<sup>3</sup> Of the types of nanomaterials, nanoparticles (NPs) in particular are a material that have at least one dimension measuring less than 100 nm, usually have a spherical shape, and have interesting optical and magnetic effects.<sup>2,4</sup> They are a naturally occurring material and can also be produced synthetically in a lab.<sup>3</sup> When researchers started examining nanoparticles more closely, it was quickly found that the size of the particles can affect the physiochemical properties of the material such as solubility, fluorescence, and optical properties. This change in properties due to their size gives nanoparticles many more functions than regular macro-sized particles. Furthermore, there are many different classifications of nanoparticles based on what chemicals they are made of: carbon-based, metal, ceramic, semiconductor, polymeric, and lipid based.<sup>2</sup>

Besides the different properties of each type of nanoparticle, the thing that makes nanomaterials an anomaly in today's society is their surface area. Nano-sized materials have a much larger surface area than larger materials such as a 1 cm cube with a similar mass.<sup>5</sup> The bigger the surface area of a particle, the greater amount of it can come in contact with other materials around it. To prove this statement, think of a cube that is 1 cm on each side which has a surface area of  $6 \text{ cm}^2$ . If that cube was filled with a bunch of tiny cubes 1 mm on each side, those would each have a surface area of  $6 \text{ mm}^2$ , which would total  $60 \text{ cm}^2$  for the entire mass taken up by the cubes. Continuing with this thought, if the original cube was filled with 1 nm sized cubes, each with a surface area of  $6 \text{ nm}^2$ , this would total  $60,000,000 \text{ cm}^2$ .<sup>5</sup> This amount is equal to  $6,000 \text{ m}^2$  which is larger than a football field. This amazing property of nanoparticles is what has

started countless studies on them and makes them useful in so many fields. Furthermore, an increase in surface area causes faster reactions and catalysis.

With all the unique properties nanomaterial have, there are a wide range of applications for them. Nanomaterials are used in the production of nanopowders for ceramics and similar materials, nanocomposites, and nanoelectrochemical systems. Nanotubes have been used for hydrogen storage, DNA chips, gene and drug targeting, nanoelectronics, and nanodevices.<sup>6</sup> Nanoparticles are used for delivery of chemotherapy drugs, to make photocatalysts, fuel cells, and solar cells. Nanowires are used in flexible solar cells, to decompose organic molecules in polluted water, and to make dense computer memory.<sup>7</sup> Some of the most ground-breaking and useful research done with nanomaterials have occurred in the biology and medical fields. Specifically, applications such as fluorescent biological labels, drug and gene delivery, bio-detection of pathogens, probing of DNA structure, tissue engineering, detection of proteins, MRI contrast enhancement, and phagokinetic studies.<sup>4</sup> The proceeding sections will discuss the idea of drug delivery more thoroughly.

Through many research projects, it has been demonstrated that nanomaterials can also be used to protect, stabilize, and preserve the activity of proteins in cells and in other materials.<sup>8,9</sup> These ideas can be used in many different areas of science. In particular, protein stabilization and delivery have important applications, such as manipulation of signaling pathways, stimulation of potent antitumor immune cells, and tissue engineering<sup>10,11</sup> These applications can be summarized as a delivery platform. Delivering proteins or drugs directly into cells can be completed in a few different ways, although, due to the size of cells, it can be a difficult task. Living organisms have cells that are generally 10 micrometers across so any form of delivery mechanism must be smaller than that.<sup>4</sup> Biological materials can be delivered into cells or other

materials using a nanoparticle as the vessel. For example, Figure 1 shows a general scheme of this delivery process of a protein transported into a cell. For this to occur, the protein (or other

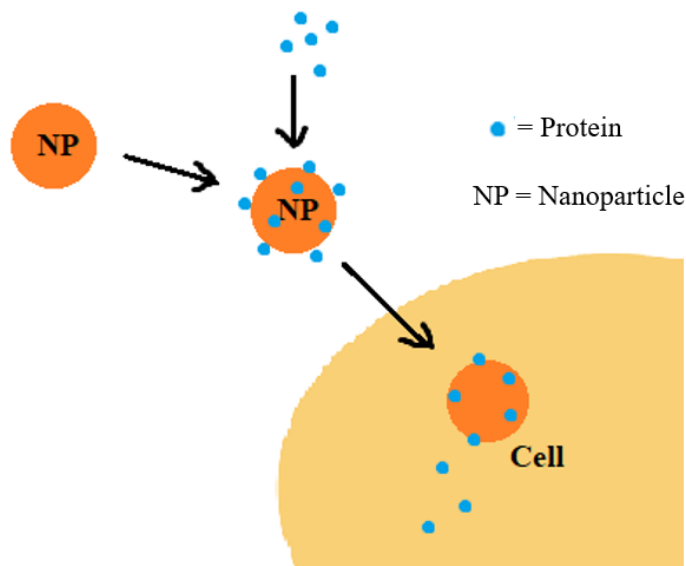


Figure 1. Transporting a protein into a cell using a nanoparticle as the transport vessel.

material) must be bound in some way to the nanoparticle for transport. In addition, there must be a transfection agent or mode of transfection for the vessel to move through the cell membrane into the cell.<sup>12</sup> Once transported into the cell, the protein will diffuse into the surrounding area by some mechanism. There are many ways for the biological material to be bound to the nanoparticle for the delivery process and many ways for it to be released into its surroundings.

Using a nanoparticle as a delivery method was first suggested in the 1970s. This idea was put into the works in 1982 where a nanoparticles were devised as a carrier for vaccines and anticancer drugs. To complete this, the research group looked at adsorbing, dissolving, or encapsulating the biomaterial to attach it to the nanoparticle.<sup>54</sup> Once the methods were working for transport, in 1997, scientists began looking at how to control the release of the drug while still protecting it from degradation. Once the 2000s came about, research groups were putting the

idea of nanoparticle drug delivery into action. In 2004, Panyam, et al. encapsulated hydrophobic drugs using biodegradable polymer nanoparticles.<sup>55</sup>

Another transport process that has been shown to work well in recent research was encapsulation. This was completed by Wurster, et al. in 2013 and involves “encapsulating” the biological material inside of the vessel before transporting. The encapsulation process can be done through many different methods, one of which is the Layer-by-Layer technique used by many research groups throughout the years which involves layering the nanoparticle vessel with many layers.<sup>12</sup> The general idea of the Layer-by-Layer method is to use a nanoparticle as the core in a delivery system. Different layers of polymers or polyelectrolytes are then added on to encapsulate a biological material such as a protein, enzyme, or nucleic acid inside the vessel.<sup>12</sup> Electrostatic interactions would hold each layer together so that each one could be taken off easily to release the biological material into the designated area. These interactions, also called van der Waals interactions, are an attractive or repulsion between two or more objects having electric charges.<sup>13</sup> Each layer must therefore be oppositely charged to bind them together since opposites attract. The weak interaction of the oppositely charged compounds is wanted so that the enzyme can be exposed to its surroundings after a time. Having a weak interaction such as the electrostatic interactions allows the release of the biomaterial to occur quickly and efficiently. Figure 2 shows a possible layering scheme that could be completed to encapsulate DNA into the vessel for delivery into a cell for gene editing.<sup>12</sup> The core would need to be a non-toxic, metal-type nanoparticle, with a stabilizing agent such as mercaptoundecanoic acid (MUA) bound to it to becoming the next layer in the encapsulation. This would cause the vessel to have a negative surface charge that would then readily bind to a positively charged polyelectrolyte such as poly(ethyleneimine) (PEI).<sup>12</sup> After the layer of PEI, the DNA can readily bind due to nucleic

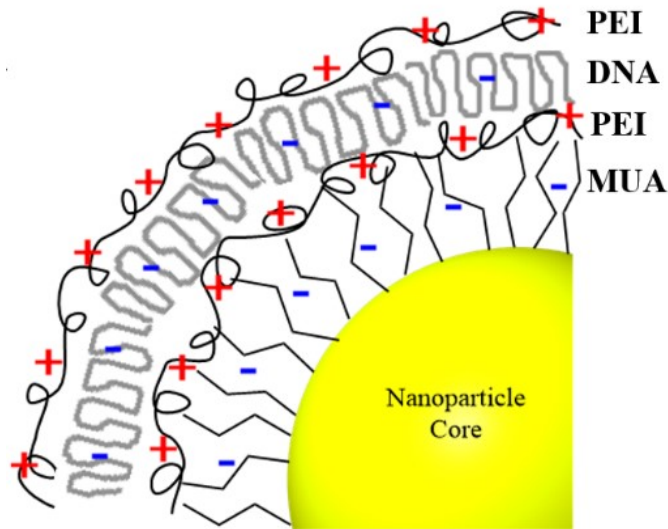


Figure 2. Order of layers for the encapsulation of DNA.

acids have strongly negative charges from their phosphate backbones. The DNA would then be the biological material being encapsulated inside the vessel for transport into the cell for biological applications. Lastly, another layer of PEI would be layered on the outside of the vessel to enclose the DNA inside and stopping it from being released too early. The positive charge of PEI would strongly bind to the negative charge of DNA holding the vessel together. PEI would be a good choice for the final layer due to it being a well-known transfection agent, meaning that it can readily pass through a cell membrane for transportation.<sup>14</sup>

With this general layering idea, nanoparticles are shown to be a good mechanism to transport biological materials into cells. Many research groups have completed this type of research making the nanoparticle system into a delivery system. It has proved to be useful, but still has a way to go. The purpose of this delivery system is for biological applications which depend on what specifically is being transported. On a genetic level, diseases such as cancer, Parkinson's disease, Alzheimer's disease, and rheumatoid arthritis are being looked at to determine pharmaceutical interventions that could potentially cure them.<sup>15</sup> Small molecules and



proteins are two possible solutions. Small molecule drugs can be transported into cells to deactivate or inhibit target proteins through competitive binding, whereas protein-based drugs can bind to a variety of targets with high specificity and can be used as substitutes for mutated or missing proteins.<sup>15</sup> These drugs however cannot target every disease-relevant protein or gene, and therefore are not always the best path to take in researching possible cures. Nucleic acids such as mRNA and DNA are another possible solution through gene editing and regulation. This is possible through specifically targeting Watson-Crick base pairing using gene editing.<sup>15</sup> Gene editing can permanently change the host's DNA which is a possible way to cure the genetic defect causing the underlying disease in question. With that in mind, nucleic acid delivery via nanoparticles is an important avenue to be explored.

## **Section 1.2 Past Research with Gold Nanoparticles**

Among the research completed on nanoparticles for drug transport, gold has been investigated intensely, specifically with the Layer-by-Layer method described in brief earlier. Gold nanoparticles have many unique properties such as size- and shape-dependent optical and electronic features, an easily modifiable surface, biocompatibility and non-toxicity.<sup>16</sup> These properties make it good for use in a living system. Gold nanoparticles also have a high affinity to interact with cells as well as to enter them.<sup>17</sup> This property, along with others, makes gold a good material for transport. The use of gold nanoparticles as a delivery method has been widely researched in the past by many groups. One in particular looked at their ability to stabilize and deliver material such as DNA, RNA, and proteins.<sup>17</sup> To set up the gold nanoparticles for delivery, they are normally stabilized by long hydrocarbon ligands to avoid aggregation. For example, mercaptocarboxylic acid can be used due to the sulfur functional group being adsorbed

by the gold surface while the carboxylic acid side points out towards the solution.<sup>17</sup> This works due to sulfur having a strong attraction to gold which binds the two materials together to form a nanoparticle conjugate for further layering.

From there, the gold nanoparticle conjugate with mercaptocarboxylic acid bound to it can be modified by binding biological molecules for delivery to it using many different methods based on the material in question: thiol-gold affinity interactions, electrostatic interactions, covalent linkage of amino groups, and physical adsorption.<sup>17</sup> The specific method to be looked at here uses electrostatic interactions and is called the Layer-by-Layer technique.<sup>12</sup> It is described as taking a nanoparticle core, encasing it with a ligand, binding the protein to that ligand, and encapsulating the final product in oppositely charged polyelectrolytes. This process produces the vessel in which the protein or material can be transported into cells for its release. Each layer is bound by electrostatic interactions from the alternative charges of each layer to make the final product one bound unit.<sup>12,17</sup> This bound unit is then the nanoparticle conjugate for the transport of biological materials.

Among the past research completed, I, along with other colleagues at Missouri State University and the University of Valladolid in Spain, published a manuscript about using gold nanoparticles as a delivery system for proteins titled *In Situ Synthesis, Stabilization and Activity of Protein-Modified Gold Nanoparticles for Biological Applications*.<sup>16</sup> The research going along with the manuscript was completed in our lab at Missouri State University. Specifically, we synthesized the delivery vessel of gold nanoparticles (AuNPs) and encapsulated lysozyme (Lys) using the Layer-by-Layer technique discussed earlier. The goal of this was to demonstrate the stability and activity of lysozyme within the nanoparticle conjugate for later adaptation for use with other proteins or biomaterials.<sup>16</sup> The layers used for this specific nanoparticle conjugate

were mercaptoundecanoic acid (MUA), polystyrenesulfonate (PSS), and polyethyleneimine (PEI) to create the oppositely charged layers for encapsulation. The order of layering was as follows: AuNPs-MUA-PEI-PSS-Lys-PSS-PEI and AuNPs-Lys-PSS-PEI.<sup>16</sup> Figure 3 is a general scheme of these experiments to produce two different AuNPs vessels for lysozyme transport. The gold nanoparticles were synthesized with  $\text{HAuCl}_4$  and a reducing agent (lysozyme or sodium citrate) prior to the layering process.<sup>16</sup> The entire procedure was completed without any activators and at near ambient conditions. To layer the particles, the Layer-by-Layer procedure discussed earlier was modified slightly to work for lysozyme as the biological material in place of DNA.<sup>12</sup> The order of layers had to be adjusted slightly due to the charge of lysozyme being positive to keep the electrostatic interactions working to bind each layer to the vessel.

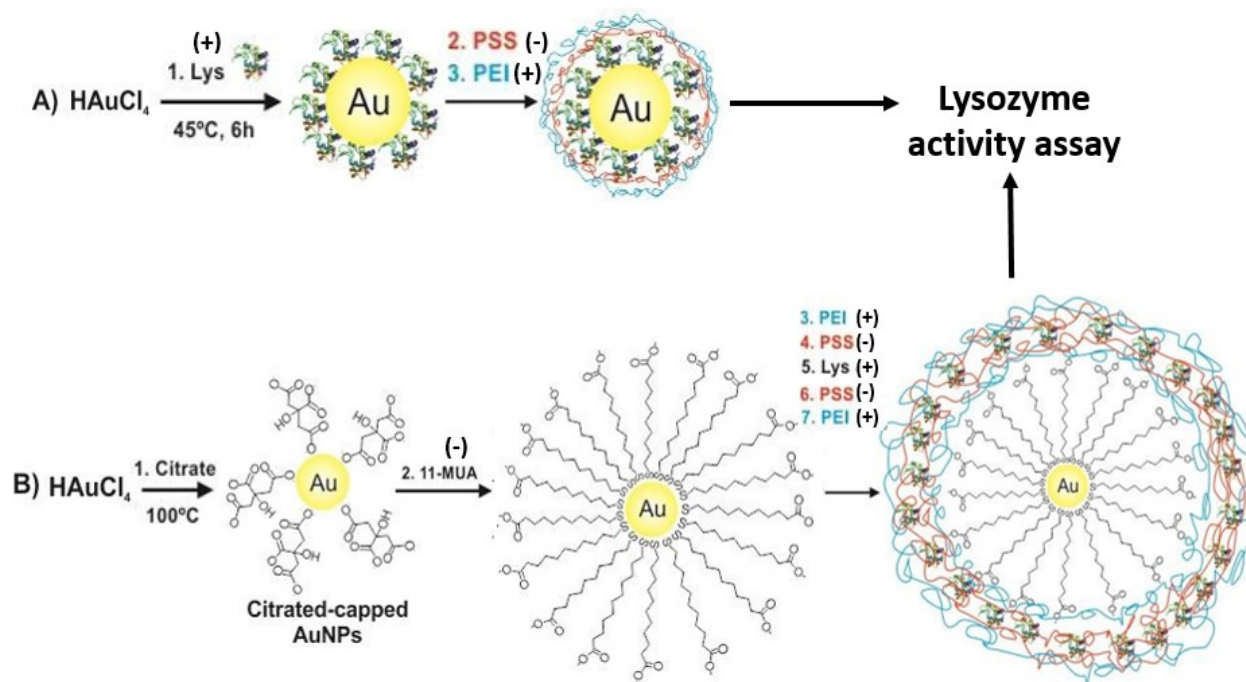


Figure 3. Methods for synthesizing gold nanoparticle conjugates showing the synthesis of Lys-AuNPs (Aa), PEI-PSS-Lys-AuNPs (Ab), citrate-AuNPs (Ba), MUA-AuNPs (Bb) and PEI-PSS-Lys-PSS-PEI-MUA-AuNPs (Bc) (Not to scale).<sup>16</sup>

After the synthesis process, characterization was completed using many techniques such as UV-Vis spectrophotometry, dynamic light scattering, electrophoretic mobility light scattering, transmission electron microscopy, Fourier-transform infrared spectrometry, as well as a lysozyme activity assay. The results from dynamic light scattering showed that after each deposition, the particles diameter increased, ending at  $\sim 130$  nm.<sup>16</sup> The zeta potential and optical properties using UV-Vis spectrophotometry were also measured and showed successful depositions after each step in the process. FTIR spectroscopy was used to assure the presence of lysozyme midway through the deposition process. With all the results obtained, it was determined that the vessel was successfully synthesized with lysozyme encapsulated inside. However, the lysozyme must be checked for its activity to make sure it was still able to be used to degrade bacteria. This was completed using *Micrococcus lysodeikticus* bacteria to observe the enzymatic action of lysozyme.<sup>16</sup> Figure 4 shows the enzymatic activity of lysozyme obtained from this research for free lysozyme and the encapsulated lysozyme nanoconjugates. It was seen that the free lysozyme reacted as predicted when added to a sample of bacteria with its activity greatly decreased from the start of the reaction reaching nearly zero activity within 12 minutes.<sup>16</sup> The layered bioconjugate samples, however, had different behaviors. These samples had an increase in activity while the outside layers were being removed from the vessel. Once the lysozyme was released into the solution of bacteria after 6 minutes for the PEI-PSS-Lys-PSS-PEI-MUA-AuNP sample, the activity began to decrease to zero in 24 minutes. On the other hand, for the PEI-PSS-Lys-AuNP sample, the activity continued increasing after 6 minutes reaching a plateau.<sup>16</sup> This shows the interaction between lysozyme and the nanoparticles actually

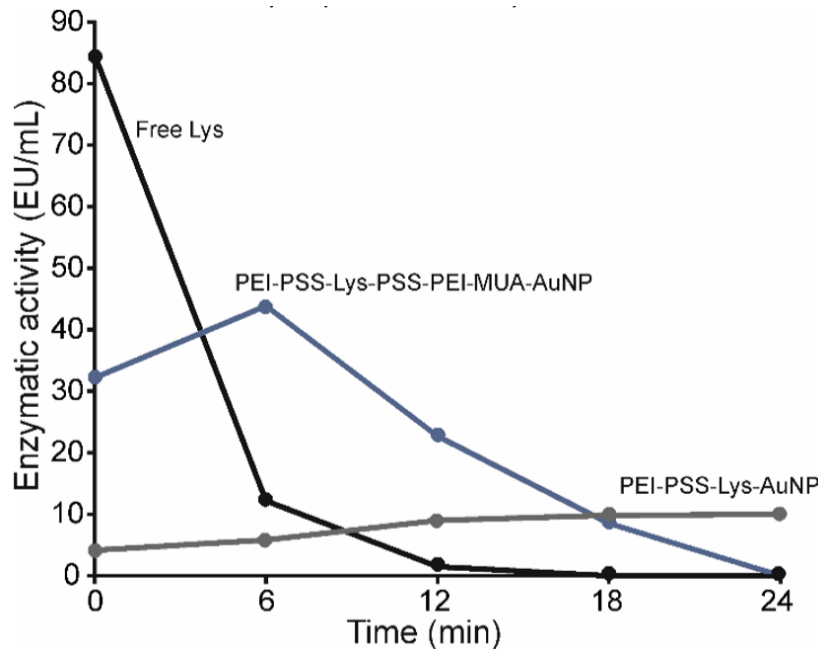


Figure 4. Enzymatic activities of free lysozyme and the lysozyme-gold nanoparticle bioconjugates expressed as  $EU/mL_{enzyme\ sample}$ .<sup>16</sup>

prolongs the activity of the lysozyme in the sample. Furthermore, these results support that the layered samples would be able to be transported into a cell before releasing the lysozyme. It also shows that the lysozyme is still able to degrade bacteria even after being encapsulated inside the vessel.<sup>16</sup>

The model protein encapsulated within the polyelectrolytes in two of the delivery systems discussed was lysozyme, 1,4- $\beta$ -N-acetylmuramidase.<sup>35</sup> Specifically, lysozyme is a small globular protein with a molecular weight of 14.6 kDa. It consists of 129 amino acid residues containing four disulfide bonds with a relatively rigid structure according to X-ray crystallography.<sup>29</sup> At physiological conditions, lysozyme is folded into a tight globular structure with a cleft on the surface of it which is its active site.<sup>35</sup> Figure 5 shows the tertiary structure of lysozyme. This enzyme is also in very high abundance in our world making it inexpensive and easily obtainable. More specifically, lysozyme is found in plants and animals, specifically in milk, tears, saliva, egg

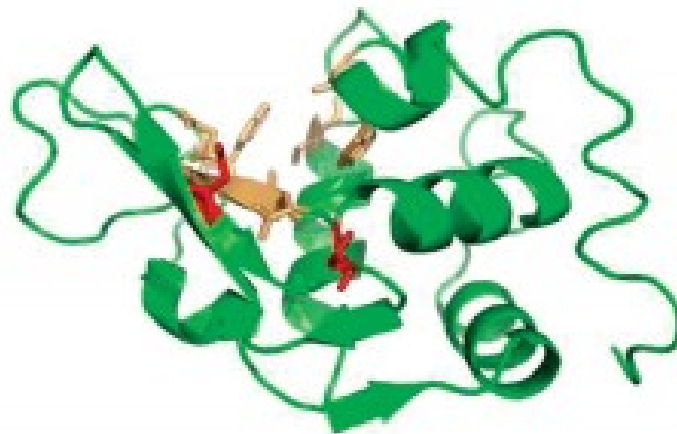


Figure 5. The tertiary structure of lysozyme with the active site shown.<sup>35</sup>

whites, and cervical mucus.<sup>35</sup> The importance of lysozyme lies in its natural antibacterial and antiviral abilities. Its function is to degrade bacteria by breaking the chemical bonds in the bacterial cell wall.<sup>35</sup>

With this project, lysozyme is a good model protein for exploring its interaction with nanoparticles and delivery systems. Furthermore, lysozyme can actually be stabilized by intermolecular electrostatic interactions.<sup>36</sup> For the encapsulation process in this research, lysozyme was bound to the delivery system in two different ways, similar to the past research completed with gold nanoparticles.<sup>16</sup> One method bound the lysozyme directly to the nanoparticle through reduction, where the other method used the stabilizing agent, MUA, between the two. The MUA binds to the lysozyme by electrostatic interactions since MUA has a negative charge from the deprotonated sulfur atom, and lysozyme has an overall positive charge due to more positive amino acids than negative ones.<sup>12,29</sup> Lysozyme also has many properties that make it ideal as a model. It is a well characterized protein with a high isoelectric point of 11.35.<sup>35</sup> In addition, lysozyme is stable over wide temperature and pH ranges, making it suitable for a variety of synthetic approaches. These properties also make lysozyme an attractive model protein for various applications. Therefore, a wide number of attempts to investigate different

ways to immobilize or encapsulate lysozyme, many of which include Layer-by-Layer steps during the process, have emerged.<sup>38,39,40</sup>

Through this research, specific polyelectrolytes were added to the nanoparticle conjugates. Polystyrene sulfonate (PSS) and polyethyleneimine (PEI) were added after the MUA and lysozyme in this case to finish the encapsulation process for later transport. PSS is a salt with a negative charge at physiological pH. PEI is a well-known transfection agent that is positive at physiological pH. These layers are attached to the conjugate by electrostatic interactions from the opposing charges between the compounds.<sup>12</sup> Figure 6 shows the branched structures of PSS (left) and PEI (right) in their general forms. At physiological pH, however, PSS has a negative charge on the oxygen atoms, and PEI will be protonated on the  $-NH_2$  groups to be  $-NH_3^+$  groups making the compound have an overall positive charge.<sup>12</sup> These charges account for how the electrostatic interactions between each layer work to bind the nanoparticle conjugate together.

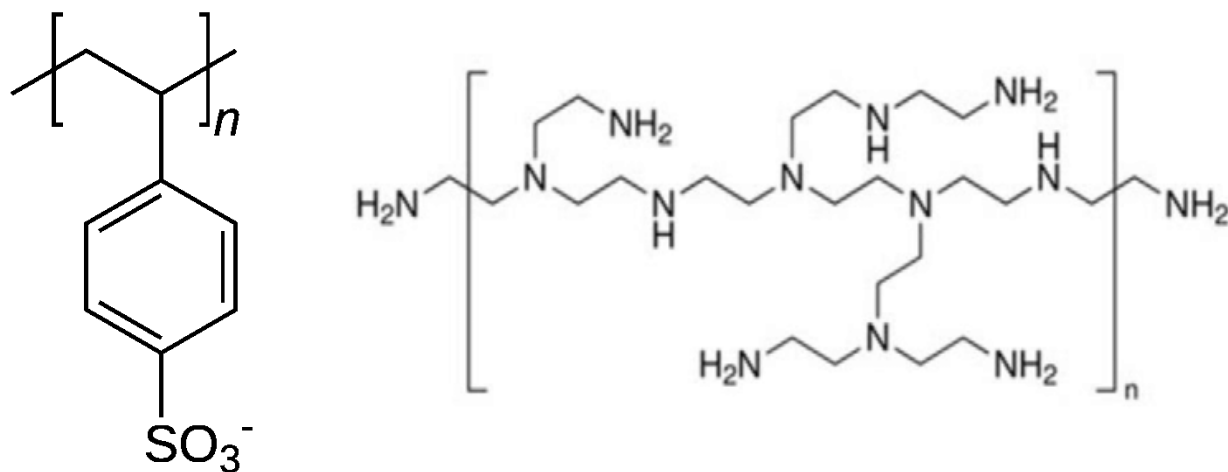


Figure 6. Polyelectrolyte branched structures of (left) PSS and (right) PEI at physiological pH.

While going through the layering process with the electrostatic interactions, there was a possibility that the nanoparticle conjugates would aggregate or be measured as a large size than expected. This could be fixed by sonication or vortexing, but sometimes there is another

phenomenon occurring that cannot be helped. Ostwald Ripening is when smaller particles within a solution attach themselves to a larger particle in order to become more stable.<sup>51</sup> This occurs because some molecules are more thermodynamically stable than others causing the unstable surface molecules to bind to larger particles in an attempt to stabilize themselves. This can also cause the particles to shrink over time due to the unstable molecules going into solution instead.<sup>51</sup> Basically, smaller particles will continue to decrease in size as parts of it go into solution due to be unstable, while larger particles continue to grow from other parts of the small molecules adding on to them. Overall, this can cause the observed diameter of the nanoparticle conjugates to be an unexpected value that is difficult to explain. Figure 7 (B) show an example of how this phenomenon occurs with smaller particles adding to larger particles to make one overall larger nanoparticle conjugate.

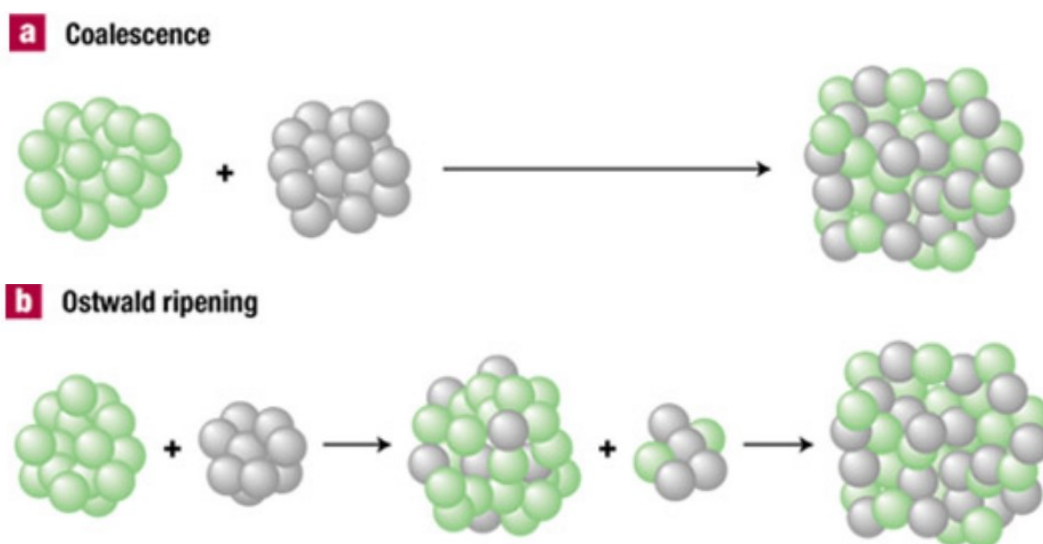


Figure 7. Examples of (A) Coalescence and (B) Ostwald Ripening to account for particle aggregating within a solution.<sup>52</sup>

Another possible cause of aggregation within the nanoparticle conjugate solution is called coalescence. Coalescence refers to overall particle growth through many stages of particle aggregation followed by grain growth.<sup>53</sup> This occurs due to the nanoparticles trying to reduce



their overall surface energy. Many research groups have monitored this event with gold nanoparticles in particular. Specifically, it has been observed that the nanoparticles start out by forming a neck with a group of particles, and then turn into a quasi-spherical shape through relaxation.<sup>53</sup> The group of particles forming the sphere then will be measured with a larger overall diameter since they are grouped together so tightly. Figure 7 (A) shows an example of how these particles group together to form an overall large diameter nanoparticle.

Overall, this research demonstrated the synthesis and stabilization of layered gold nanoparticles at near ambient conditions.<sup>16</sup> Lysozyme was successfully encapsulated into the vessel for later transport into cells via transfection. This research project was done specifically for lysozyme, looking at its stabilization and activity throughout the experiment. Lysozyme was used as a model in this protocol and could readily be modified for the transport of other proteins or biological materials.<sup>16</sup> This research also demonstrated that nanoparticles, gold in this specific case, can be used as the core in the encapsulation process of a biological material for transport into cells. More specifically, nanoparticles can be used as a delivery system for drugs as well as other materials. With this project being used as a guide, much more can be done in this field with nanomaterials and delivery systems. Both the nanoparticle core and the biological material encapsulated can ideally be interchanged with other compounds and materials for further investigation of this process.

One such biomaterial that can be swapped for lysozyme is ribonucleic acid. Ribonucleic acid (RNA) is one of the major biological macromolecules found in all known life forms.<sup>41</sup> It is similar in structure to deoxynucleic acid, DNA, but has one more –OH group attached to the ribose ring. Furthermore, RNA is single-stranded unlike DNA. Figure 8 shows a simple backbone structure of a strand of RNA. It has a backbone with alternating ribose, which is sugar,

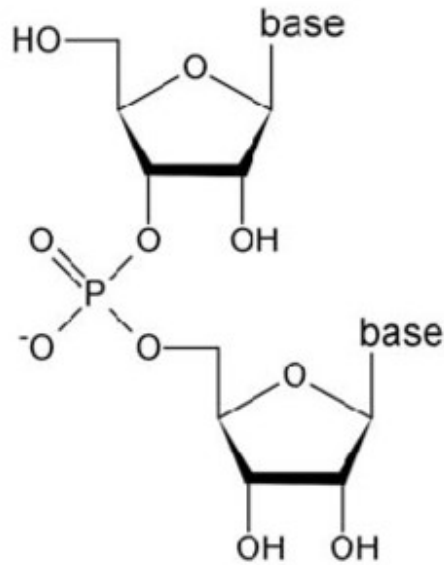


Figure 8. General Structure of Ribonucleic Acid.

and phosphate groups. Then, attached to each ribose is one of the four possible bases: cytosine (C), guanine (G), adenine (A), or uracil (U).<sup>42</sup> The negative charge on the phosphate groups accounts for the overall negative charge on the structure. There are also different types of RNA within each cell. Specifically, there is messenger RNA, ribosomal RNA, and transfer RNA to list a few. Small RNAs have been found to be useful in gene expression and gene editing over the past several years.<sup>42</sup> Specifically, the RNA sequence could silence gene replication by binding to the end of another sequence. With that in mind, encapsulating RNA in the nanoparticle conjugate can therefore be used for gene regulation once transported into the cell.

Once encapsulated inside the nanoparticle conjugate, the RNA must still be intact to be useful for gene regulation. If the RNA degrades, it will break into nucleotides becoming ineffective for targeting genetic mutations.<sup>43</sup> Just like with lysozyme, once the encapsulation process is completed with RNA successfully in the nanoparticle conjugate, its integrity must be tested to assure that it is still intact and able to be used for gene regulation in the future. To do this, an ethidium bromide assay can be used with measuring fluorescence to determine if the

RNA is degraded or not.<sup>44</sup> Ethidium bromide is an intercalating agent, meaning it inserts itself between the planar compounds in other molecules. It is commonly used as a fluorescent tag with DNA or RNA, which is its purpose here. Ethidium bromide binds readily to intact RNA and becomes very fluorescent. If the RNA is degraded, however, the fluorescence of the RNA will greatly decrease the fluorescence of the bound ethidium bromide due to it being fragmented.<sup>45</sup> This causes the binding affinity of ethidium bromide to the sequence to greatly decrease. That being said, the fluorescence is a good determining factor to show whether the RNA is intact.

To compare the encapsulated RNA to intact RNA and degraded RNA, a sample of RNA must be degraded before having its fluorescence with ethidium bromide tested. There are many laboratory methods for degrading RNA such as adding a strong base, reducing the pH to below 4 with an acid, or heating it above 120°C for a certain amount of time.<sup>43</sup> Each of these methods causes RNA to be unstable and degrade over time. Degraded RNA will not be useful as a drug. For the ethidium bromide assay, two of these methods were used to degrade a sample of intact RNA to determine its fluorescence when bound to RNA.<sup>44</sup>

### **Section 1.3 Zinc Oxide Nanoparticles**

Although the research with gold was promising, the chemicals needed to synthesize gold nanoparticles are expensive. Looking at alternative nanomaterials, zinc oxide (ZnO) is a common inorganic, semiconducting compound with a wide band gap of 3.37 eV that has been found to form nanostructures under certain conditions.<sup>21</sup> It is insoluble in water and has an extremely high melting point of 1975°C. In nature, it occurs in the mineral zincite, but is usually synthesized for industrial uses.<sup>22</sup> The compound has three different crystalline forms that it exists in: salt, wurtzite, and zincblende. These are shown in Figure 9. Of synthesized zinc oxide, the wurtzite

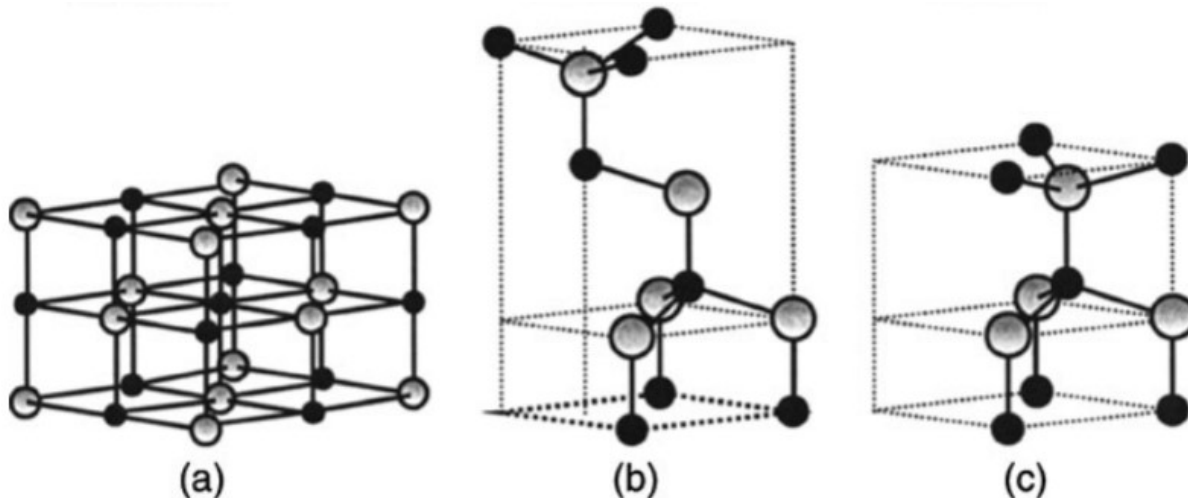


Figure 9. Common Zinc Oxide Crystal Structures of (a) cubic rock salt, (b) cubic zincblende, and (c) hexagonal wurtzite where grey and black spheres represent zinc and oxygen atoms respectively.<sup>22</sup>

structure is observed more often due to it being more stable under ambient conditions.<sup>22</sup>

Recently, zinc oxide has emerged into the nanotechnology field for various applications. Before then, it was well-known for its uses in electronics, optics, photonics, and rubber industries.<sup>22,23</sup> In the 1960s, films of zinc oxide were being synthesized to be used in sensors, transducers, and catalysts. When nanotechnology started breaking scientific barriers, the zinc oxide films were looked at more closely and could be synthesized as nanowires which could be used to make the thin films in question.<sup>24</sup> Reducing the compound to nano-size brought about many new surface and optical properties that widened its uses in products.<sup>23</sup>

In regard to its use as a delivery system, zinc oxide has a few special abilities, such as anticancer and antimicrobial activities, which make it a useful drug carrier.<sup>25</sup> Zinc oxide has actually been used in many health care products due to its efficient antimicrobial activity against gram-positive and gram-negative bacteria. Research has been done to show the possible mechanisms of this phenomenon such as the formation of reactive oxygen species or the release of  $Zn^{2+}$  ions. Both cause damage to the bacteria cell membrane through various interactions.<sup>26</sup>

Zinc oxide nanoparticles are also more affordable to synthesize than gold nanoparticles, as well as many other nanoparticles, needing only two common compounds.<sup>26</sup>

Zinc oxide nanoparticles have been shown to be potentially useful in nano-medicine and biomedical sciences at select doses, although the toxicity is still being looked at by many research groups<sup>28</sup>. Specifically, one study showed that injecting enough zinc oxide into mammalian cells to cause bactericide did not have any cytotoxic effects on the mammalian cells.<sup>26</sup> Another important characteristic of zinc oxide is its ability to interact with enzymes, especially lysozyme.<sup>27</sup> It has been shown in past research that zinc oxide is capable of disrupting protein-protein associations by binding to the protein in question.<sup>29</sup> The zinc oxide nanoparticle can bind to the largest cleft on the lysozyme surface, while retaining the secondary structure of the enzyme. This also causes the protein to maintain its enzymatic activity, even under denaturation.<sup>29</sup>

Through many research projects in the past decades, zinc oxide has been found to be a versatile functioning material due to it having a wide range of growth morphologies besides the general nanowires and nanoparticles: nanocombs, nanorings, nanohelices, nanobelts, and nanocages.<sup>23</sup> Each morphology of the zinc oxide nanostructures has different physical and chemical properties specific to it.<sup>21</sup> This also helped widen the possible uses of zinc oxide nanomaterials. Some important applications of zinc oxide that have emerged through the years are UV-light emitters, surface acoustic wave devices, ceramic varistors, transparent high-power electronics, piezoelectric transducers, and catalysis via gas sensing.<sup>30</sup>

Today, there are many different methods in the literature for synthesizing zinc oxide nanostructures. Some, but not all, are laser ablation, thermal decomposition, co-precipitation, hydrothermal methods, ultrasound, electrochemical depositions, anodization, combustion

method, sol-gel method, and chemical vapor deposition.<sup>21</sup> Some synthetic processes can be controlled to produce different morphologies such as solution concentration, pH, washing medium, and chemical compounds used.<sup>21</sup>

Examining the precipitation methods, zinc oxide can be synthesized using multiple combinations of compounds. Combining sodium hydroxide with either zinc chloride, zinc acetate, or zinc nitrate will precipitate zinc oxide.<sup>27,31</sup> The following reaction in Figure 10 shows how zinc oxide is precipitated using zinc chloride as the zinc source.<sup>32</sup> Some literature states that



Figure 10. Reaction for the synthesis of zinc oxide nanoparticles.

this reaction occurs in multiple steps with zinc hydroxide,  $\text{ZnOH}_2$ , being an intermediate, and then the hydrogens being removed when drying the solid sample to form the final product of zinc oxide,  $\text{ZnO}$ . The trick to making the particles nano-sized is the conditions in which they are synthesized. The solutions must be added together dropwise to have a very slow, regulated reaction to form the zinc oxide precipitate. Ideally, the longer the reaction, the smaller the particles will be.<sup>31</sup> The solution must also be stirred strongly for the entire time of the addition of the compounds. The other factors affecting the size of the particles are the temperature at which they are synthesized, and how long the reaction takes place. Heating the particles at  $90^\circ\text{C}$  will give a spherical shape, causing them to be smaller, while heating at  $45^\circ\text{C}$  will cause nanorods to form instead.<sup>27</sup> When combining these reactants, it is possible to form zinc hydroxide instead of zinc oxide. UV-Vis spectroscopy can be used to assure that the proper compound was synthesized. Zinc oxide is known to absorb at  $\sim 360\text{ nm}$  which is a quick, efficient way to test for the product.<sup>32</sup>

The past research with gold can be adapted to use zinc oxide instead. The binding method must be investigated to assure the layering will occur. One of the layers used in past research was mercaptoundecanoic acid (MUA) which is a stabilizing agent and gives the nanoparticle conjugate a negative surface charge that will readily bind to lysozyme.<sup>16</sup> This is due to the MUA having a negative charge on the sulfur atom after deprotonation at physiological pH. Gold has been shown to readily bind to the sulfur in MUA due to gold having a high affinity for sulfur. The sulfur will readily bind to the gold interface forming gold thiolate bonds. It is hypothesized that zinc interacts the same way, even with the oxide on it. Figure 11 gives a general scheme of how these bonds are hypothesized to occur. The  $Zn^{2+}$  will have a surface interaction with the sulfur atom on the MUA to bind the nanoparticle to that ligand.<sup>34</sup> Another hypothesized method

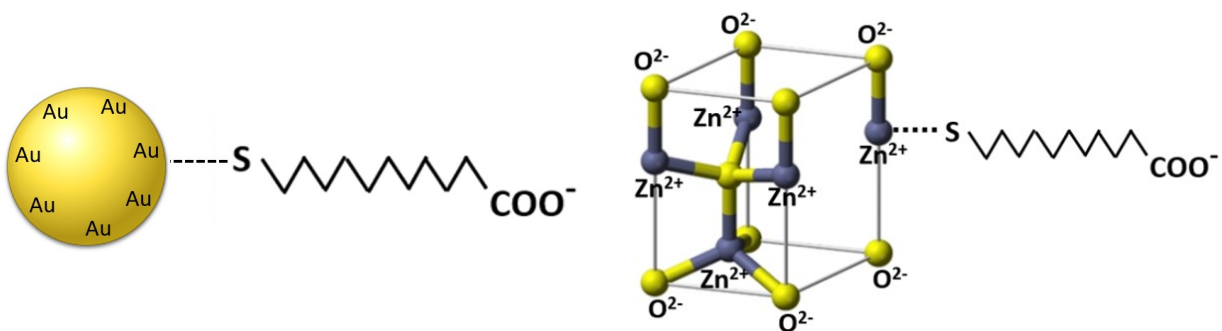


Figure 11. Binding Mechanisms of gold (left) and zinc (right) to MUA.<sup>33</sup>

of the binding of zinc oxide to sulfur is that the wurtzite crystal structure of zinc oxide has oxygen vacancies. The sulfur atoms can then fill these vacancies and bind to the zinc in oxygen's place.

Furthermore, when binding the nanoparticle directly to the biological material lysozyme in past research, the gold nanoparticles were synthesized with lysozyme as the reducing agent. If zinc oxide is used instead of gold, the binding mechanism changes. When looking at the surface charges of lysozyme and zinc oxide, they are both positive. With that in mind, it seems that these

will not bind through electrostatic interactions as the rest of the layers do. However, that is actually incorrect. Lysozyme has two catalytic residues in its binding site, Glu35 and Asp52.<sup>29</sup> These amino acids are negatively charged at physiological pH which causes the binding site to be negatively charged. With zinc oxide having a positive surface charge and the binding site on lysozyme having a negative charge, electrostatic interactions do account for the binding mechanism between the two materials.<sup>29</sup>

### **Section 1.4 Motivations**

The past research with gold nanoparticles used as a vessel for transporting biological material into a cell was a good starting point for delivery systems. Further research can be completed to optimize the results and the system overall. The motivations of this research are to develop a new nanoparticle conjugate system for drug delivery and show proof of concept by changing the encapsulated material. Zinc oxide nanoparticles are more affordable to synthesize and purchase than gold nanoparticles. This will allow the synthesis process to be more cost effective. The procedures used by two different groups for layering, Wurster and et al. and Garcia and et al., were modified for this project with zinc oxide to encapsulate lysozyme and RNA in the nanoparticle conjugates for future transport into cells.<sup>12,16</sup> Lysozyme was encapsulated first to assure that the process would work with a model protein before moving on to less stable biological materials such as RNA.

Overall, the synthesized nanoparticle conjugates would be another method for drug delivery. This is a more specific way to deliver medicine to a certain area in the body. Furthermore, gene regulation would be an end goal to potential fix gene mutations, cure diseases, or produce proteins.



## Section 1.5 Objectives

The main goals of this research project:

1. To synthesize and characterize zinc oxide nanoparticle bioconjugates
2. To verify the biological activity of the zinc oxide nanoparticle bioconjugates

Three nanoparticle bioconjugates were synthesized and characterized: ZnO-Lys-PSS-PEI, ZnO-MUA-Lys-PSS-PEI, and ZnO-MUA-PEI-RNA-PEI. With all this completed, the different orders of the layering process were compared between all three systems. Furthermore, these bioconjugates could potentially be used to transport the encapsulated material into mammalian cells to destroy unwanted bacteria or edit mutated genes causing diseases.

## CHAPTER 2. EXPERIMENTAL

### Section 2.1 Materials

All chemicals and solvents were reagent grade and used without further purification. Poly(ethyleneimine) (branched, 25 kDa), poly(sodium 4-styrenesulfonate) (branched, 70 kDa and 1000 kDa), 11-mercapto-undecanoic acid, (MUA), Lysozyme (Lys) from chicken egg white, bacteria *Micrococcus lysodeikticus*, Corning® syringe filters membrane (with diameter 15 mm and pore size 0.2  $\mu\text{m}$ ), and RNA from torula yeast, type VI, were purchased from Sigma-Aldrich (St. Louis, MO, USA). Poly(ethyleneimine) (branched, 60 kDa) was purchased from Acros Organics. Zinc chloride anhydride was purchased from Alfa Aesar. Sodium hydroxide and sodium chloride were purchased from Fisher Scientific. Sodium citrate dihydrate and sodium phosphate monobasic were purchased from Spectrum Chemical Manufacturing Group (Gardena, CA, USA). Sodium phosphate dibasic was purchased from Mallinckrodt Chemical Works (St. Louis, MO, USA). The ethidium bromide was borrowed from Dr. Udan's laboratory in the Missouri State University Biology Department. Deionized water with a resistivity of 18.2  $\text{M}\Omega\cdot\text{cm}^{-1}$  was used to prepare all the solutions.

### Section 2.2 Methods

Many instruments and techniques were used in the synthesis and characterization of the zinc oxide nanoparticle conjugates. Purification of zinc oxide nanoparticle suspensions was performed using a micro-centrifuge (D3024 from Scilogex, Rocky Hill, CT, USA). Once purified, multiple instruments were used to characterize each sample. X-ray diffraction (XRD) was used to determine the crystal structure of the zinc oxide nanoparticles. Dynamic Light

Scattering (DLS) and Electrophoretic Mobility Light Scattering (ELS) were used to measure the diameter, polydispersity, and zeta potential of the particles before and after deposition (NanoBrook Omni from Brookhaven Instruments, Holtsville, NY, USA). For particle sizing measurements using the DLS, the samples were re-suspended in 1 mM NaCl and filtered with a 0.2  $\mu\text{m}$  corning filters. Purified samples did not need to be filtered for zeta-potential purposes but were re-suspended in 1 mM NaCl. An UV-Vis spectrophotometer was used for optical properties and for the enzymatic activity assays (Cary-60, Agilent Technologies, Santa Clara, CA, USA). Absorbance spectra were recorded from 200 to 800 nm. Size measurements and images were obtained using a Scanning Electron Microscope (SEM) (Quanta 200 FEG, Oxford Instruments). FTIR spectroscopy was used to obtain the transmittance spectra for the samples (Vertex 70, Bruker). Finally, fluorescence spectroscopy was used for the ethidium bromide assay with the RNA samples to test the nanoparticle conjugates integrity (Horiba Scientific, QM-8075-21-C). Purification was completed as stated above before each analysis to assure the sample was not contaminated. Sonication and/or vortexing was also completed after each purification step to assure the particles were well dispersed and not aggregated within the sample.

**Section 2.2.1 Dynamic light scattering spectroscopy.** Dynamic Light Scattering (DLS) is a characterization technique used by many research groups to analyze particle size.<sup>12</sup> For this research, it is an analysis method to determine if each layer was added to the bioconjugate. This instrument measures the dynamic diameter and polydispersity of the particles in a conductive solution. Polydispersity is the measure of non-uniformity of the particles, so a lower polydispersity value is better. To find the diameter of the particles, a laser is passed through the sample which scatters off the particles at different angles and intensities.<sup>18</sup> The equation to calculate the diameter is called the Stokes-Einstein Equation and is as follows:  $D_h = \frac{k_B T}{3\pi\eta D_t}$

where  $D_h$  is the hydrodynamic diameter,  $D_t$  is translational diffusion coefficient,  $k_B$  is Boltzmann's constant,  $T$  is temperature, and  $\eta$  is the dynamic viscosity.<sup>18</sup> Using that equation, the diameter of the particles can be determined which allows for further analysis to see if the particles in question are nano-sized, and if each deposition is successful. A general scheme of how the DLS instrument works is shown in Figure 12. This instrument works very well as long as the particles are not aggregated, or clustered, within the sample. Aggregation of nanoparticles can be avoided by making sure the particles are at a particular temperature, pH, or lighting, as well as being in the proper solvent. If the particles do aggregate, it can be helped with sonication or vortexing.

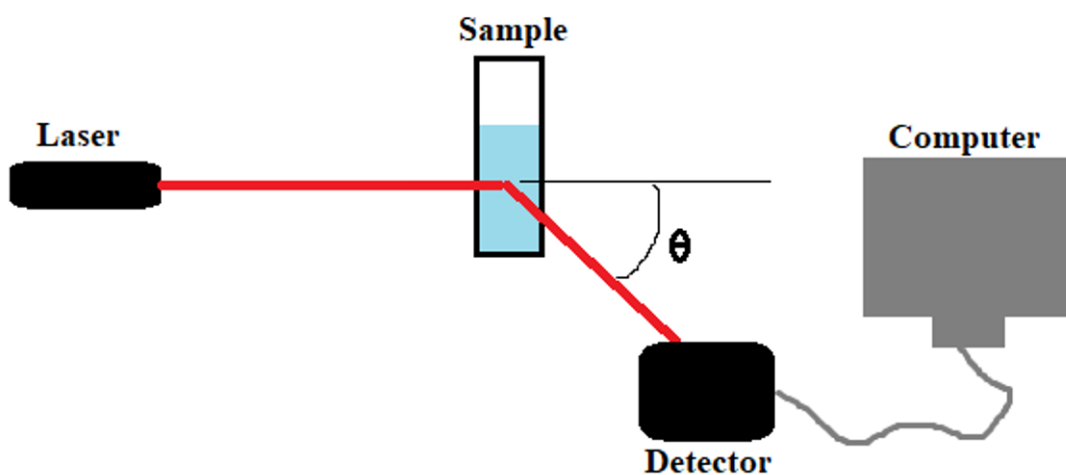


Figure 12. General Scheme of Dynamic Light Scattering Instrument.

**Section 2.2.2 Electrophoretic mobility light scattering spectroscopy.** Another major technique used in the previous research was Electrophoretic Mobility Light Scattering (ELS) to determine the zeta potential of the particles after each deposition.<sup>12</sup> This analysis helps to determine if each layer was bound successfully to the nanoparticle conjugate due to the charges alternating which each deposition through the layering process. Zeta potential is the potential difference between the surface of the particle and the conducting liquid it is immersed in.<sup>19</sup> This

can be determined through light scattering and creating a potential within the sample. An electrode is placed in the sample to create the potential difference which will move the charged particles to their respective sides—opposites attract. The light scattering is completed to determine the electrophoretic mobility of the charged particles.<sup>19</sup> It is then used to calculate the zeta potential through the following two equations summarized as the Smoluckowski Equations:  $\mu = \frac{v}{V L}$  and  $\zeta = \frac{\eta \mu}{\epsilon}$  where  $\mu$  is the electrophoretic mobility,  $\epsilon$  is dielectric constant,  $\zeta$  is zeta potential,  $\eta$  is dynamic viscosity,  $v$  is the speed of the particle,  $V$  is the voltage, and  $L$  is length of the electrode.<sup>19</sup> The general scheme of how the ELS works is shown in Figure 13.

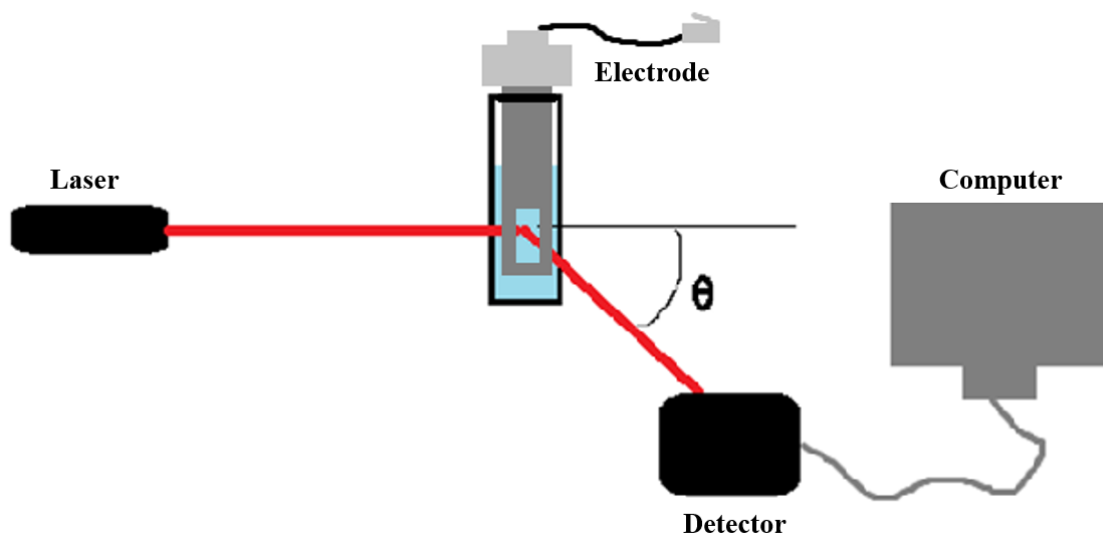


Figure 13. General Scheme of Electrophoretic Mobility Light Scattering Instrument.

While doing experiments with this instrument, it was found that there is no universally accepted standard for ELS measurements.<sup>20</sup> While looking into what may work as a standard, an inexpensive option that would work for the negative and positive ranges was found: Coffee Mate coffee creamer. At an acidic pH at or below 3.0, this coffee creamer has a positive zeta potential, and at a basic pH above 7.0, it has a negative zeta potential.<sup>20</sup> Between those pH values, it gives

a neutral zeta potential reading around 0.0 mV. With these findings, Coffee Mate could be used as the standard for the later experiments taking place.

When investigating this possible standard, to assure that the expected values were obtained, multiple trials for the positive and negative standards were completed and are shown in Figure 14. To begin, a phosphate buffer containing KCl at pH 8.0 was made for the negative standard, and a citric acid buffer at pH 3.0 was made for the positive standard. Then, about 5 mg of Coffee Mate coffee creamer was dissolved in 10 mL of the respective buffer. Each sample was sonicated thoroughly to assure the sample was fully dispersed and then brought to the ELS for measuring. For each trial, a fresh sample must be made. If left for multiple days, the Coffee Mate coffee creamer standard becomes contaminated and no longer charged. After testing thirteen fresh samples for each standard, the positive standard was averaged at  $32.88 \text{ mV} \pm 2.90$  and the negative standard at  $-39.90 \text{ mV} \pm 3.84$ . The graphs shows each trial for both standards measured with the ELS. With these standards, each use with the ELS can be assumed to be correct as long as the proper values are being measured for these standards. Furthermore, these

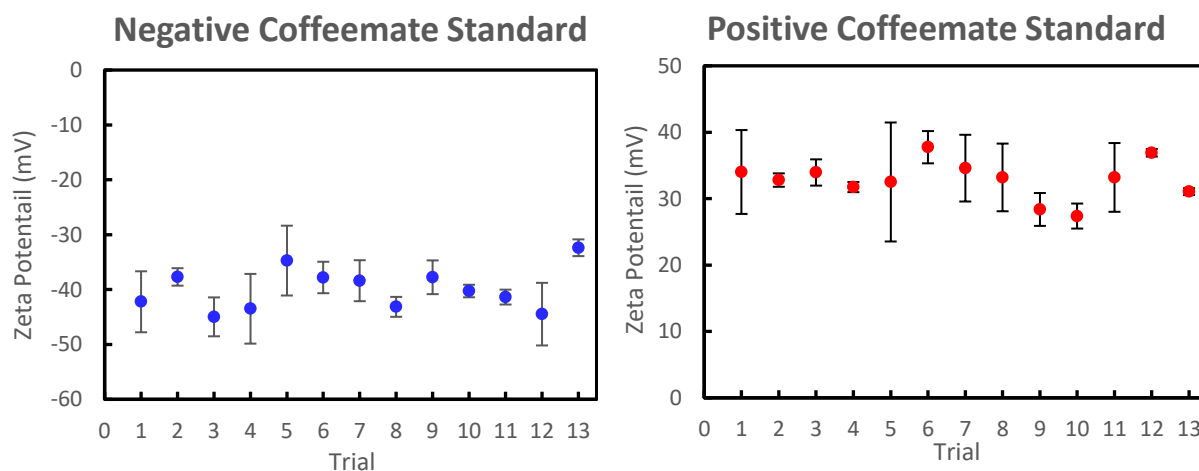


Figure 14. Coffee Mate Standards for ELS with negative values on the left and positive values on the right.

results show that zeta potential of a substance can be dependent on pH in certain cases. This must be considered when comparing literature values with experimental ones in future analyses.

### **Section 2.3 Synthesis of PEI-PSS-Lys-MUA-ZnO NPs**

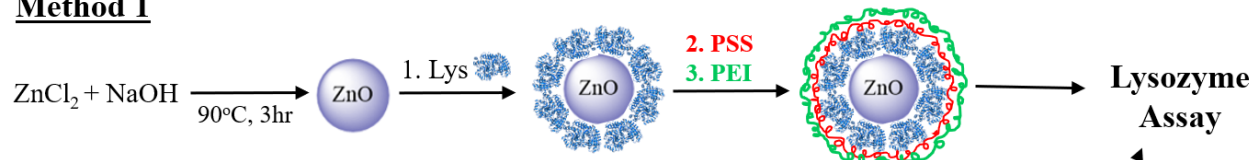
Zinc oxide nanoparticles were synthesized in the presents of mercaptoundecanoic acid to obtain the core and first layer of the desired vessel as shown in Figure 15 (Method 2). This synthesis was completed using a modified version of a well-known method called Layer-by-Layer.<sup>12</sup> To begin, 20 mL of 0.05% ZnCl<sub>2</sub> was heated at a constant 45°C while stirring at 300 rpm. Then, 0.02 g of MUA was dissolved in 10 mL of 0.02 M NaOH by heating and stirring. This solution was then added dropwise to the stirred solution of ZnCl<sub>2</sub>. It was left to react with heating and stirring for various amounts of time ranging from 1 to 24 hours to vary the size of the particles. The reaction was cooled to room temperature. The sample was washed and purified using a centrifuge at 5000 rpm for 5 minutes. The sample was washed with deionized water once and then resuspended in 1 mM NaCl.

Two different orders of layering can be completed with the MUA-ZnO NPs to form Lys-PSS-PEI-MUA-ZnO NPs and Lys-MUA-ZnO NPs. The one used here was Lys-MUA-ZnO NPs to reduce the overall number of layers being added to the vessel. The other method would ideally be just as useful, but more time consuming. For the layering process, a 10 mg·mL<sup>-1</sup> lysozyme solution in phosphate buffer solution (pH 7.00) was added dropwise to the stirred solution of purified MUA-ZnO NPs at ambient conditions. The final concentration of lysozyme in the solution was 60 μM. The particles were purified as stated before and layered with PSS (1000 kDa). A solution of 10 mg·mL<sup>-1</sup> PSS in deionized water was added dropwise to a stirred solution of Lys-MUA-ZnO NPs at room temperature to end with a final concentration of 2 mg·mL<sup>-1</sup> of

PSS. Then, after washing, a solution  $10 \text{ mg}\cdot\text{mL}^{-1}$  PEI (60 kDa) in deionized water was added dropwise to a stirred solution of PSS-Lys-MUA-ZnO NPs at room temperature to end with a final concentration of  $2 \text{ mg}\cdot\text{mL}^{-1}$  of PEI. The PSS-PEI-MUA-ZnO NPs could be layered according to the above procedure, just with a different order of layers. Each sample would be sequentially layered as stated above to form PEI-PSS-Lys-PSS-PEI-MUA-ZnO NPs and PEI-PSS-Lys-MUA-ZnO NPs.

Characterization would take place after each layering procedure using DLS, ELS, FTIR spectroscopy, and UV-Vis spectrophotometry for these nanoparticle conjugates. Each sample would be washed and purified, resuspended in 1 mM NaCl, and then analyzed with each instrument. After all the layering was completed, the starting material, ZnO-MUA nanoparticles, and the final layered nanoparticle conjugates were observed and imaged using the SEM. These

### **Method 1**



### **Method 2**

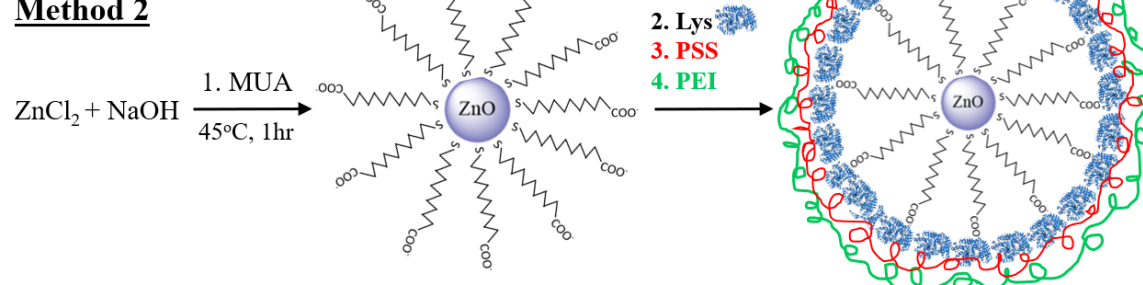


Figure 15. Methods for synthesizing zinc oxide nanoparticle conjugates without the use of a stabilizing agent (Method 1) and with the use of the stabilizing agent MUA (Method 2).



images were then compared to examine the difference in the particles before and after the layering process. Enzymatic activity assays were completed following all other characterization techniques.

#### **Section 2.4 Synthesis of PEI-PSS-Lys-ZnO NPs**

Zinc oxide nanoparticles were synthesized in a different fashion for the addition of lysozyme directly to the nanoparticles as shown in Figure 14 (Method 1).<sup>27</sup> A 500 mL, three-neck round bottom flask was placed in a heating mantel. Each spout was filled as follows: a thermometer for temperature control was placed in the left-neck with a rubber septum; a condenser with a KIM wipe loosely stoppering the top was placed in the middle-neck to control evaporative effects; a 150 mL separatory funnel was placed in the right-neck with a rubber septum. Then, 50 mL of 1.00 M NaOH was put inside the flask with a stir bar. The flask was heated to a temperature of 90°C with stirring at 400 rpm. Next, 50 mL of 0.50 M zinc chloride was placed in the separatory funnel for slow addition to the flask. Once the NaOH reached its desired temperature, the zinc chloride solution was added dropwise very slowly to the solution. It took approximately 45 minutes for all of the zinc chloride to be added. The solution was allowed to sit for an additional two hours to finish reacting. The resulting precipitate was filtered using a vacuum pump and a filter flask. It was washed with several portions of deionized water and then removed from the funnel with the filter paper. The resulting solid was placed in the oven at 60°C for one day to dry it out.

From there, the layering could proceed. To add the first layer, 5 mg·mL<sup>-1</sup> of lysozyme was placed in a centrifuge tube with 100 µL of phosphate buffer (pH 7.00) and 900 µL of deionized water. The absorbance was measured at 280 nm and recorded. Then, 10 mg·mL<sup>-1</sup> of

the synthesized ZnO NPs were added to the centrifuge tube and incubated from one day then centrifuged for ten minutes at 13,000 rpm. The absorbance of the solution was taken again to determine if the lysozyme binded to the ZnO NPs. The resulting Lys-ZnO NPs were purified by centrifugation at 5000 rpm, washed with deionized water, and resuspended in 1 mM NaCl as described above. The coating of Lys-ZnO NPs with PSS and PEI was completed using the same techniques as for the MUA-ZnO NPs for a final product of PEI-PSS-Lys-ZnO NPs.

Just like the nanoparticle conjugates of ZnO-MUA, these conjugates were characterized using DLS, ELS, FTIR spectroscopy, and UV-Vis spectrophotometry after each deposition took place. Each sample was washed, purified, resuspended in 1 mM NaCl, and then analyzed as before. After all the layering was completed, the starting material of ZnO nanoparticles and the final nanoparticle conjugates were observed and imaged using the SEM. These images were then compared to see the difference between the starting material and final product.

## **Section 2.5 Lysozyme Activity Assay**

The residual activity of the lysozyme within the layered nanoparticle conjugate was tested using a lysozyme activity assay with the UV-Vis spectrophotometer.<sup>16</sup> Bacteria *Micrococcus lysodeikticus* was used as a substrate for the enzymatic action of lysozyme. The concentration of encapsulated lysozyme was determined spectrophotometrically using an extinction coefficient of  $2.63 \text{ mL} \cdot \text{mg}^{-1} \cdot \text{cm}^{-1}$  when measuring the absorbance at 280 nm. This value is most likely the same for encapsulated lysozyme due to it having the same properties in and out of encapsulation. *Micrococcus lysodeikticus* solution was prepared by dissolving 50 mg of bacteria in 100 mL of 50 mM buffer phosphate (pH 6.25). The ZnO NPs samples and free lysozyme were dissolved in 50 mM buffer phosphate (pH 6.25) each. 600  $\mu\text{L}$  of the sample was

added to 3 mL of bacteria solution at room temperature and mixed. The decrease in the absorbance was monitored continuously at 600 nm for 30 minutes at room temperature. The enzymatic activities were determined from the slope of the fitted line when representing the absorbance decay plots and using the following equation:

$$\frac{\text{Units}}{\text{mL}_{\text{enzyme sample}}} = \frac{(\Delta Abs_{600} / \text{min test} - \Delta Abs_{600} / \text{min blank})}{0.001 \times 0.6}$$

where 0.001 is the change in the absorbance per minute for lysozyme, and 0.6 is the added volume of sample to the bacteria solution during the tests measured in mL<sup>16</sup>. The blank used for the assays was 50 mM phosphate buffer. The residual activity (%) was calculated as the ratio of the activity at time *t* to the initial activity multiplied by 100.

From there, the residual activities calculated from each sample were graphed vs. time and compared to the free lysozyme sample. These activities can also be compared to other nanoparticle conjugates to determine how effective the order of layering and residual activities were. In addition, it can be hypothesized whether or not these particles would work for the transport into cells when looking at these results.

## Section 2.6 Synthesis of PEI-RNA-PEI-MUA-ZnO NPs

For the encapsulation of RNA instead of lysozyme, the same layering procedure was completed but using a sample of RNA instead and a different order of layers.<sup>12</sup> For this experiment, the ordering of layers was ZnO-MUA-PEI-RNA-PEI for the final nanoparticle conjugate as shown in Figure 16. The ZnO-MUA nanoparticles were synthesized slightly different from the procedure described before. Instead, 50 mL of 1.0 M NaOH was heated in a flask to 90°C. While heating, 0.04 g of MUA was added to the flask and dissolved. After this solution reached its designated temperature, 50 mL of 0.5M ZnCl<sub>2</sub> was added using a separatory

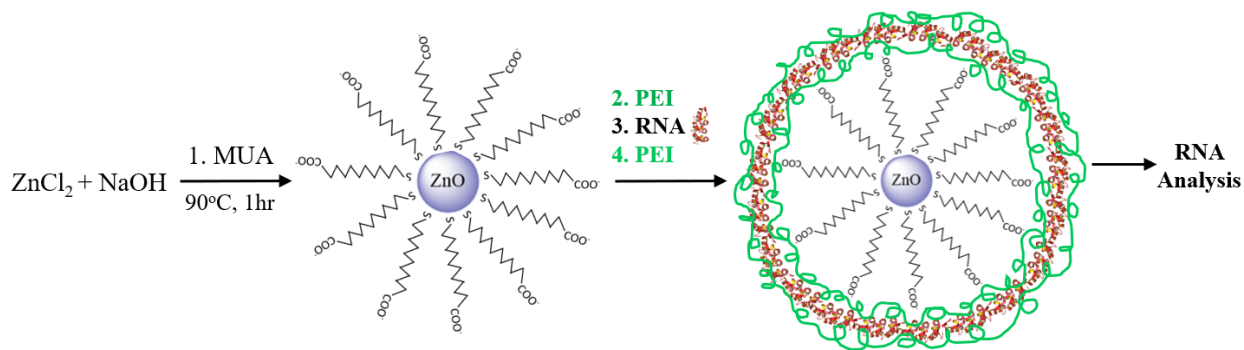


Figure 16. Encapsulation of RNA method for synthesizing zinc oxide nanoparticle conjugates with the stabilizing agent MUA.

funnel. The zinc chloride was added dropwise over a period of about an hour. Once the addition was over, the solution was removed from heat, washed, and resuspended in 1mM NaCl for further layering.

The first layer of PEI (25 kDa) was added as before starting with a 10mg/mL stock solution and adding it dropwise to the nanoparticles for a final concentration of 1mg/mL. The sample was washed and purified as before with DI water and centrifugation, and resuspended in 1mM NaCl. The RNA was added next according to the Layer-by-Layer technique discussed earlier.<sup>12</sup> A stock solution of 1mg/mL RNA was made with DI water and stored in the fridge when not in use. This sample was added dropwise to the stirred solution of ZnO-MUA-PEI nanoparticles for a final concentration of 0.2 mg/mL. It was left to stir for 30 minutes at room temperature to bind and stabilize. The sample was then washed and resuspended in 1mM NaCl for the last deposition step. The last layer of PEI was added exactly as before with a final concentration of 1mg/mL. The resulting particles were stored without washing, with excess PEI in solution, for multiple weeks for testing. When ready to analyze, the particles were washed and resuspended in 1mM NaCl.

Again, the nanoparticle conjugates were characterized using DLS, ELS, FTIR spectroscopy, and UV-Vis spectrophotometry after each deposition process. Each sample was washed, purified, resuspended in 1 mM NaCl, and then analyzed. After the entire layering process was finished, the starting material of ZnO-MUA nanoparticles and the final layered nanoparticle conjugates were observed and imaged using the SEM. The starting material and final product could then be compared for differences as well as compare these samples to the ones with encapsulated lysozyme.

### **Section 2.7 RNA Integrity Analysis**

The RNA integrity analysis was completed by addition of ethidium bromide and measuring the resulting fluorescence of the solution. To begin the ethidium bromide assay, a sample of free RNA was used to determine the difference in absorbance between an intact RNA strand and a degraded RNA strand.<sup>44</sup> For this test, 970  $\mu\text{L}$  of 230  $\mu\text{g}/\text{mL}$  RNA in 0.1 M PBS buffer at pH 7.4 were added to two separate test tubes.<sup>45</sup> Then, 29  $\mu\text{L}$  of 500  $\mu\text{g}/\text{mL}$  ethidium bromide was added for a final concentration of 36.9  $\mu\text{M}$  in PBS buffer at pH 7.4.<sup>46</sup> These two samples were covered in foil to protect the ethidium bromide from reacting with the light, which would reduce its affinity to bind to RNA. To degrade one of the RNA samples, two methods were attempted. First, a couple drops of 0.1 M HCl was added to the test tube and mixed. The second method involved heating the original sample to 120°C in a water bath for approximately 10 minutes. Following each degradation process, a color change was observed from pink to a faint orange. The fluorescence was then measured for the two samples to assure that the degraded sample would have a lower fluorescence. It was measured with an excitation wavelength of 510 nm with a length of 520 nm to 700 nm for both test tubes.<sup>44</sup>

Following that procedure, the nanoparticle conjugate sample was tested the same way. To begin, 480  $\mu\text{L}$  of 0.1 M PBS buffer at pH 7.4, 480  $\mu\text{L}$  of purified ZnO-MUA-PEI-RNA-PEI nanoparticles, and 15  $\mu\text{L}$  of 500  $\mu\text{g}/\text{mL}$  ethidium bromide were pipetted into two test tubes.<sup>45</sup> Both tubes were mixed well and covered with foil. These samples had the same pink color as the nondegraded standard RNA samples. Then, a couple drops of 0.1 M HCl were added to one of the test tubes to attempt to degrade the RNA in the sample. In addition, the process was repeated with the other degradation method of heating the sample to 120°C for 10 minutes in a water bath. Both methods showed the samples quickly turn from pink to orange just like the standard samples. From there, all the samples had their fluorescence tested with an excitation wavelength of 510 nm and measured from 520 nm to 700 nm.<sup>44</sup> The fluorescence of the nondegraded sample and the degraded one could then be compared to see if there was a difference.

### CHAPTER 3. RESULTS AND DISCUSSION

After synthesizing each nanoparticle conjugate encapsulating one of the two biological materials, characterization was completed to ensure that each layer was successfully bound to the layer before through electrostatic interactions. Furthermore, the biological material was checked for its activity to assure that it was still useful for cell transport once encapsulated. This section describes the results and interpretations obtained from each instrumental analysis before, during, and after the deposition process for each nanoparticle conjugate sample. Furthermore, these results will be discussed and compared to determine the effectiveness of these experiments.

X-ray diffraction was used to confirm the crystal structure of the synthesized zinc oxide nanoparticles used for all of the following layering techniques. Figure 17 shows the XRD pattern of the sample. When compared to literature patterns of XRD for different crystal structures, this

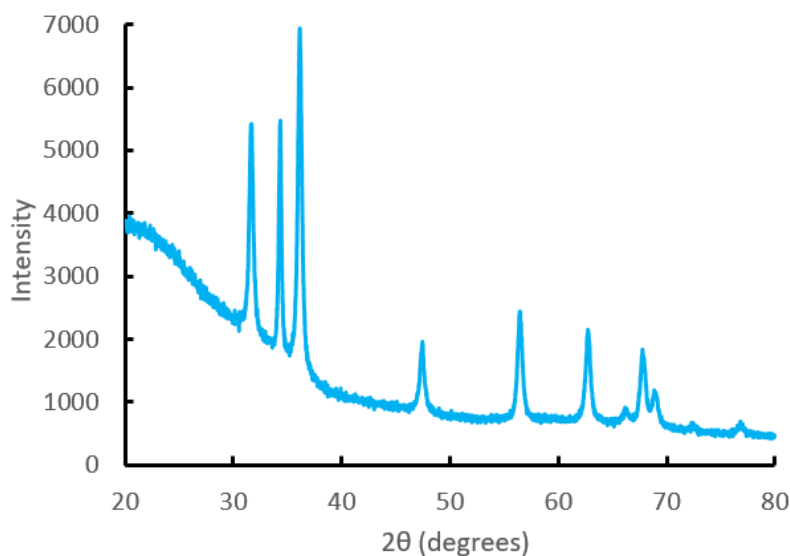


Figure 17. XRD pattern of synthesized zinc oxide nanoparticles.

pattern shows the wurtzite structure as hypothesized.<sup>56</sup> The specific peaks confirming this are the three between 30 and 40 degrees, one at 47 degrees, and one at 56 degrees. In addition, due to it

being a bulk sample with particles at about 200 nm in diameter, there are some extra peaks visible which can be attributed to this.

### **Section 3.1 Encapsulation of Lysozyme**

The following sections discuss the results for the encapsulation of lysozyme with the same techniques and ordering of layers as the past research with gold nanoparticles. The two methods were compared along the way for similarities, differences, and which method worked better.

**Section 3.1.1 UV-Vis Spectrophotometry.** When layering the zinc oxide nanoparticles, an absorbance spectrum was obtained after each layer to show the basic composition of the solution using the UV-Vis spectrophotometer. All three orders of layering were analyzed after each deposition from the original nanoparticle sample to the final nanoparticle conjugate with the encapsulated biological material. The absorbance was measured from 200 to 800 nm with 1 mM NaCl being used as the blank. Some of the compounds used in this experiment have known absorbance peaks that can be used to identify and confirm their presence in the solution containing the nanoparticle conjugates. Specifically, zinc oxide is known to absorb light at 360 nm providing a strong peak at that wavelength depending on the concentration of it.<sup>31</sup> This is the main peak observed in each absorbance spectrum due to zinc oxide being the core of the conjugate. Further analysis involves the known absorbance of lysozyme at 280 nm due to the amino acids present in its structure, and the absorbance peaks of PSS observed at 260 nm and 228 nm.<sup>12,16</sup> From here, the absorbance of each sample was measured and observed.

Figure 18 shows the absorption spectra of the synthesized ZnO-MUA nanoparticles after each layer was added for a final product of ZnO-MUA-Lys-PSS-PEI. The major peak being



looked at is the one at 360 nm for the starting material of zinc oxide that did not have MUA as a stabilizing agent in its synthesis procedure. This peak confirms the presence of zinc oxide in the solution. To add the first layer, MUA, to the nanoparticles, zinc oxide was synthesized with MUA in the solution. Due to this, the peak at 360 nm was greatly decreased in size due to the outer most layer of MUA being at such a high concentration. Continuing in the deposition process, the characteristic absorbance peak of lysozyme was observed at 280 nm. The characteristic absorbance peak of PSS is also well seen when it is the outside-most layer at 260 nm. Although the zinc oxide peak at 360 nm should be more visible in each spectrum, the overall data does confirm the presence of each deposition layer. The concentration of MUA was adjusted for further synthesis processes with the other nanoparticle conjugates so that the zinc

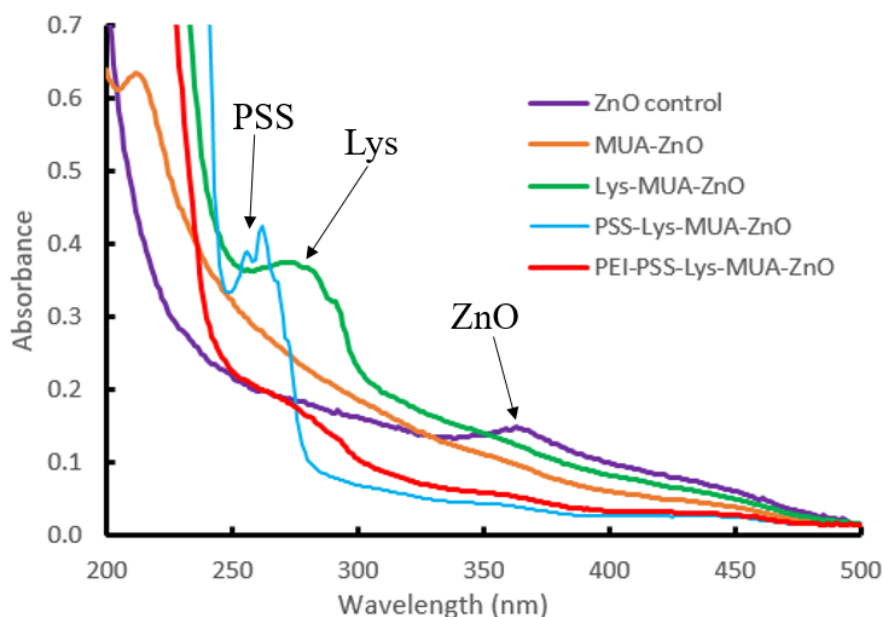


Figure 18. Absorbance Spectra for ZnO-MUA-Lys-PSS-PEI layered nanoparticle samples after each deposition.

oxide peak was visible through each deposition. Overall, for this sample, each deposition was successful, and these results with the model protein of lysozyme were used to optimize the later synthesis and encapsulation of RNA in the nanoparticle conjugates.

The absorbance spectra for the ZnO-Lys-PSS-PEI samples were also obtained and are shown in Figure 19. After each deposition, the absorbance was measured from 200 to 800 nm with the blank being 1 mM NaCl as with the other samples. The characteristic zinc oxide peak was seen in all spectra at 360 nm which was expected due to the MUA not being present. This result is the goal for the RNA encapsulated nanoparticle conjugates completed following this

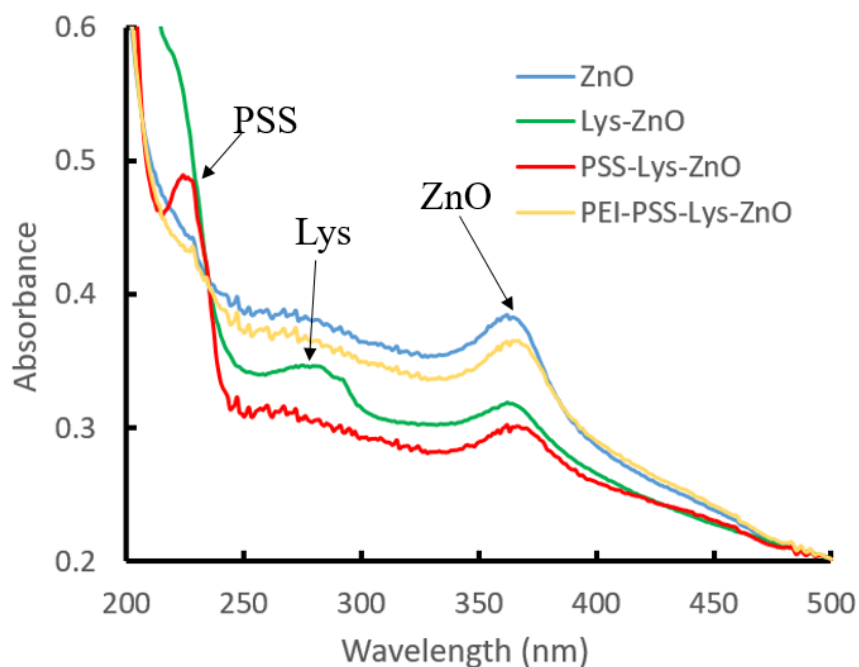


Figure 19. Absorbance Spectra for ZnO-Lys-PSS-PEI layered nanoparticle samples after each deposition.

experiment. Specifically, the concentrations of  $ZnCl_2$  and NaOH to synthesize the zinc oxide nanoparticles described in the experimental sections were used for the synthesis of ZnO-MUA nanoparticles for the RNA encapsulation process. From there, the lysozyme peak was observed at 280 nm as expected in the next spectrum. The characteristic PSS peak is also seen well at about 230 nm. This absorbance is different than the previous sample but it is due to the PSS having an overall different concentration. PSS absorbs at both 260 nm and 228 nm, but whether both peaks are observed depends on how dilute the solution is. In brief, these spectra do show the

presents of the zinc oxide and lysozyme as was predicted. It can be concluded with this preliminary data that each layer did bind to the nanoparticle conjugate to form the overall vessel with lysozyme encapsulated inside. These results compared to previous with MUA used as a stabilizing agent were looked at, and the methods were actually combined to synthesize and characterize the last nanoparticle conjugate with RNA.

**Section 3.1.2 Scanning Electron Microscopy.** Due to the very small size of the nanoparticle conjugates, hence the “nano” in the name, microscopy was used to observe each sample. Specifically, a scanning electron microscope was used to image and observe the size and morphology of the zinc oxide nanoparticles before and after the deposition process. With these images, the general size and shape of the particles was observed. To begin, the ZnO-Lys-PSS-PEI nanoparticle conjugates were evaluated. Figure 20 (A) shows the synthesized zinc oxide nanoparticles before any depositions took place. They have a spherical shape although it was not uniform across the whole film. The size of each particle was estimated at 150 nm using the scale

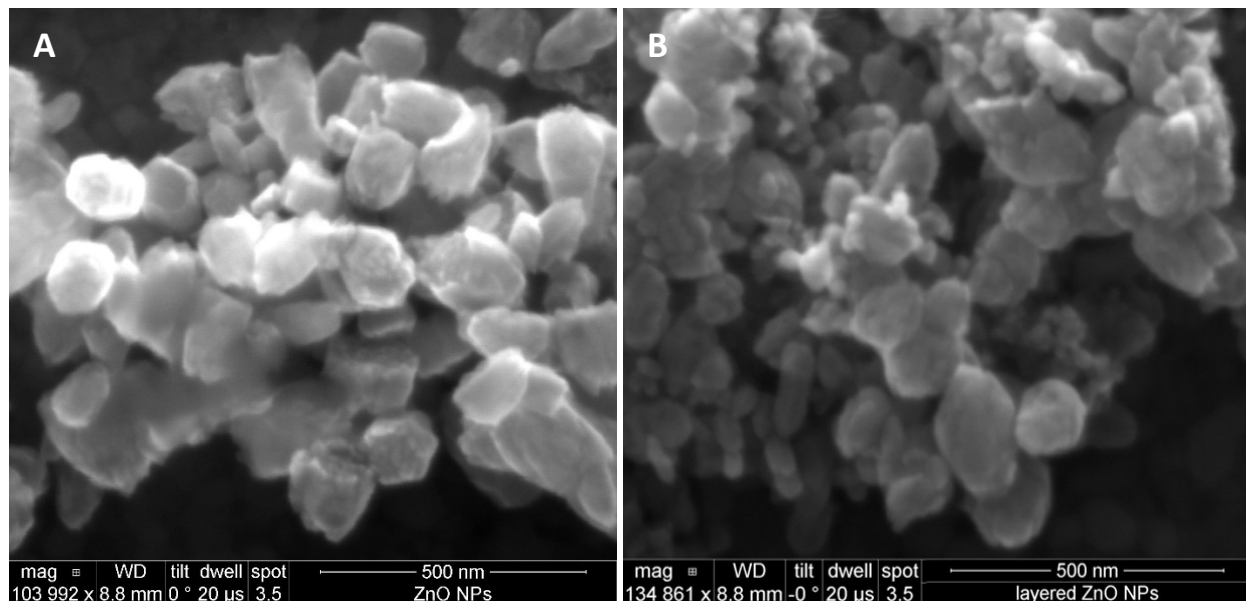


Figure 20. SEM images taken for the ZnO-Lys-PSS-PEI NP samples (A) before and (B) after deposition with the scale bar in the right corner of each to estimate the size of the particles.

bar in the lower right corner of the image. Figure 20 (B) has the ZnO NPs after the deposition process, specifically for the ZnO-Lys-PSS-PEI ordering. These particles were observed to be 250 nm, although the size and shape varied greatly between each particle as seen in the image. Furthermore, these particles were much more aggregated after the layering process took place. Comparing both images, the particles did increase in size after the layering process as expected, and the shape remained mostly spherical after all the layers were added.

The second method for synthesizing the nanoparticle conjugates to encapsulate lysozyme used MUA as a stabilizing agent in the synthesis of the zinc oxide nanoparticles. The deposition process was analyzed just as before with the SEM imaging the particles before and after the process was completed. Figure 21 (A) shows the particles before deposition took place which is for the ZnO-MUA NP sample. These particles were shown at about 200 nm in diameter and were mostly spherical, although some rough edges were observed accounting for the crystal structure of wurtzite.<sup>22</sup> Figure 21 (B) shows the nanoparticle conjugates after deposition with a final

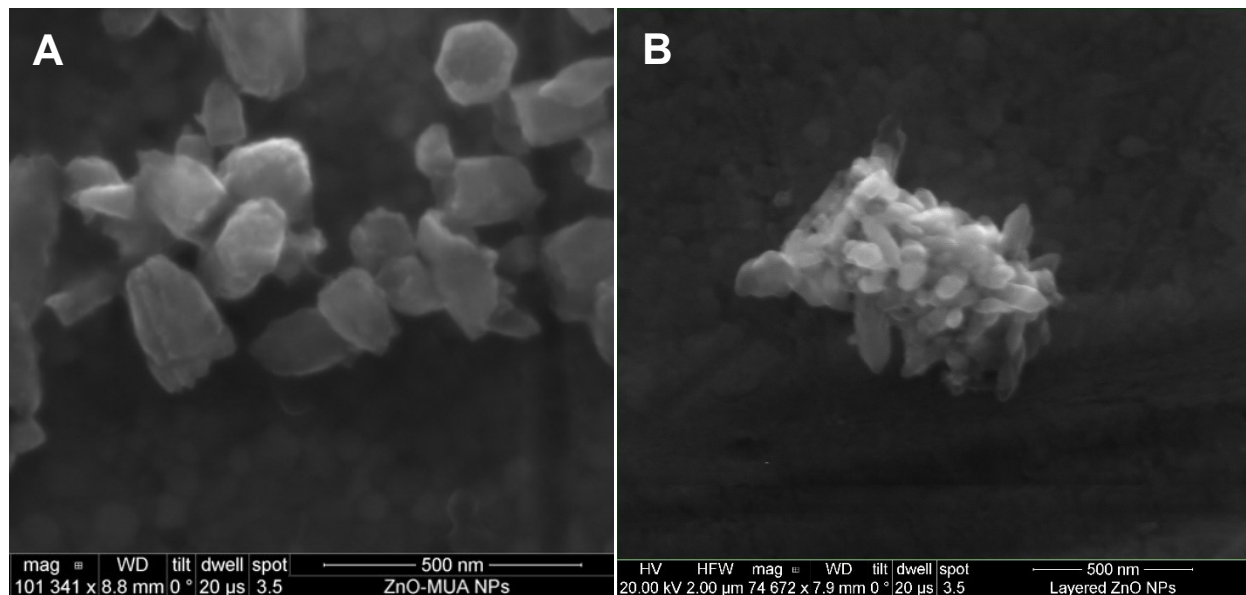


Figure 21. SEM images taken for the ZnO-MUA-Lys-PSS-PEI NP samples (A) before and (B) after deposition with the scale bar in the right corner of each to estimate the size of the particles.

ordering of layers as follows: ZnO-MUA-Lys-PSS-PEI. These particles ranged from about 400 nm to 500 nm and became more aggregated. As seen in the image, the particles started to acquire needle-like structures on the outside of the spheres during the layering process. Overall, these particles increased in size as expected with layers being added to them.

To sum up, this section shows how the nanoparticle conjugates were hypothesized and confirmed to increase in size after the deposition process was completed. Adding layers to the original particles should increase the size after each layer was added, so these results are encouraging. Further sizing measurements with the DLS were taken though to confirm this hypothesis.

**Section 3.1.3 Dynamic Light Scattering.** When beginning the synthesis process for the zinc oxide nanoparticles, many well-known methods have been used to synthesize them by themselves. However, adding MUA into the solution to bind the ligand onto the outside of the nanoparticle while synthesizing the nanoparticle in question creates a new protocol to optimize. This new protocol would involve synthesizing ZnO-MUA nanoparticles all at once. The parameters of the protocol from synthesizing the particles with and without MUA in the solution were all the same to begin with except for the time allowed for the reaction to occur. With MUA present, the reaction time was varied from 1 hour to 24 hours, with the diameter of the particles being measured immediately after synthesis and washing. Figure 22 shows the diameter of the zinc oxide nanoparticles versus the reaction time to compare the differences observed. As shown by the graph, as reaction time increases so does the diameter of the nanoparticles. At a reaction time of 1 hour, the nanoparticles averaged 170 nm, while at 24 hours had a diameter of about 290 nm. Any size of these nanoparticles would be useful in this research, but it is helpful to be able to

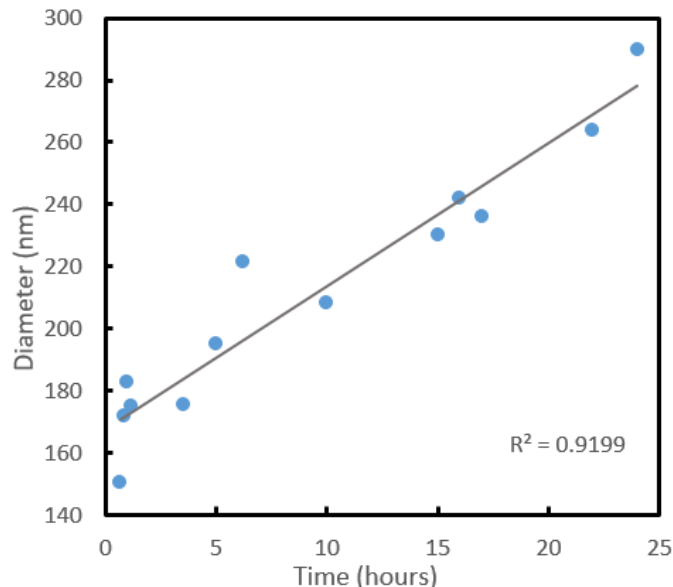


Figure 22. Nanoparticle diameter versus reaction time for the synthesis of zinc oxide nanoparticles coated with MUA.

predict the size of the nanoparticle conjugates based on the initial reaction time. The goal would also be to use the smallest possible nanoparticle size for further research.

Although using the SEM to estimate the size of the nanoparticle conjugates was useful, it was not enough to settle with just these results. To determine the exact diameter of the nanoparticles throughout the synthesis and layering process, Dynamic Light Scattering spectroscopy (DLS) was used after each step. After each deposition, the diameter and polydispersity of the nanoparticle samples were measured. Multiple trials were completed for each layering order starting with the synthesized zinc oxide nanoparticles and ending with a layer of PEI. The trials involved making a completely new sample of nanoparticle conjugates for each measurement process. These diameters could then be compared to the estimated values observed from the SEM. With both measurements, the size of the nanoparticles can be confirmed. Furthermore, the polydispersity shows how uniform the particle size is across the sample. Ideally, this value should be low.

For the first sample of ZnO-MUA-Lys-PSS-PEI, the size and polydispersity is shown in Figure 23 after each layer averaging four trials. The polydispersity is also seen on the right axis of this graph. The particles started at 159 nm after the synthesis of the original zinc oxide nanoparticle with MUA in the solution. Moving to the next layer with lysozyme, the size greatly increased to 368 nm which was higher than expected. With the addition of PSS, the size actually

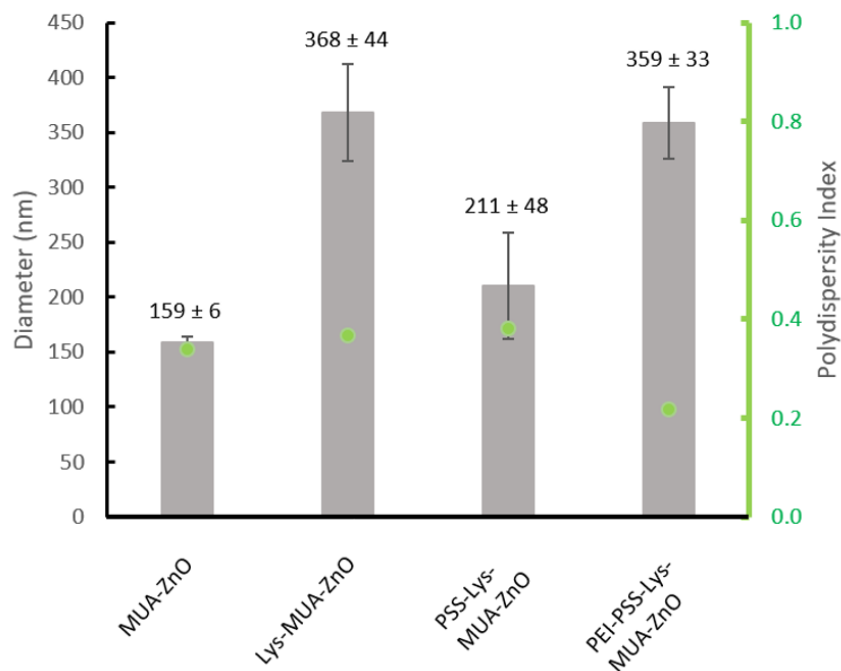


Figure 23. Particle diameter (left axis) and polydispersity (right axis) of ZnO-MUA-Lys-PSS-PEI conjugates measured with the DLS with mean and standard deviation labelled.

decreased to 211 nm which is about where the particle size was expected to be at this point. The decrease in size for this deposition is hypothesized to be due to the electrostatic interactions.

Going from the positive lysozyme step to a negative PSS layer, if the concentrations of each were high enough, the attraction would have been very strong between the two. This could have pulled the final layer even tighter towards the core of the conjugate to cause a decrease in the diameter. Furthermore, it also could have been Ostwald Ripening or nanoparticle coarsening.<sup>51,53</sup>

The final layer of PEI increased the size of the conjugate to an ending diameter of 359 nm. The

polydispersity varied from about 0.2 to 0.4 throughout the layering process showing that the particle size was well dispersed throughout the solution. In brief, these results do match the estimated values from the SEM being within 50 nm each.

For the next ordering, the zinc oxide was bound directly to the lysozyme layer without any stabilizing agent for a final ordering of ZnO-Lys-PSS-PEI. The diameter and polydispersity were also measured for this sample after each deposition and is shown in Figure 24 for an average of four trials. The synthesis of these particles started out as just zinc oxide with no other layers added unlike the previous sample. The starting diameter of the ZnO was 124 nm. With each deposition, these particles increased in size as expected. The lysozyme layer increased the diameter to 210 nm, PSS layer to 297 nm, and the PEI layer to a final size of 323 nm. The polydispersity decreased with each layer, meaning the particles became more uniform in their size throughout the deposition process ending at about 0.16. Again, these results with the DLS

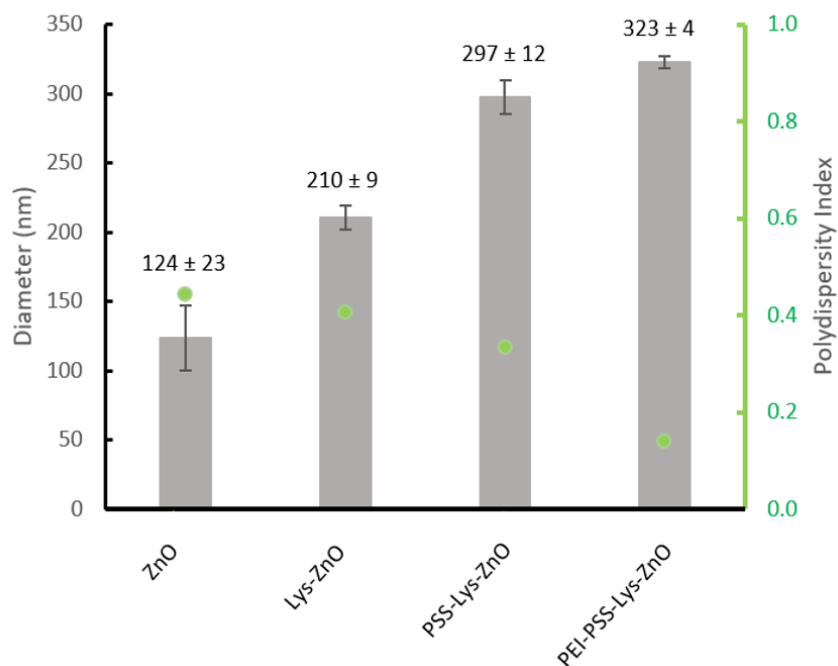


Figure 24. Particle diameter (left axis) and polydispersity (right axis) of ZnO-Lys-PSS-PEI conjugates measured with the DLS with mean and standard deviation labelled.



were compared to the ones from the SEM. The SEM showed that the particles were slightly smaller in the end than the DLS measured, however were still somewhat close. This difference in measurements could have been due to aggregation between the particles causing a larger reading from the DLS.

With these results from the SEM and the DLS, the size of the nanoparticle conjugates can be confirmed to be nano-sized and verified as the values seen above. The diameter steadily increased with each deposition as hypothesized ending at a size ranging from 300 to 400 nm. Any non-consistent values of increasing diameter can be attributed to Ostwald Ripening or coarsening causing the nanoparticles to shrink and grow in an unpredictable manor.<sup>51,53</sup> Although much larger than the gold nanoparticle conjugates this research is based off of, these nanoparticle conjugates can still be used for drug delivery and could be reduced in size by adjusting some of the parameters in future experiments.

**Section 3.1.4 Electrophoretic Mobility Light Scattering.** Along with measuring the diameter of the particles, the zeta potential was also measured after each deposition to assure each layer did bind as expected. The layers interact through electrostatic interactions from their oppositely charged surfaces. Therefore, when looking at the zeta potential after each deposition, if the next layer binds, the surface charge measured should switch to the opposite charge, and therefore be alternating with each measurement. Each nanoparticle conjugate sample was measured to determine the surface charge after each deposition. The zeta potential values for the layers without the nanoparticle conjugates are shown in Table 1 to the what charge is expected for each layering.<sup>16,47,48</sup> The exact value depends on the concentration of the compound as well as the pH at which the measurement was taken. This is why it will vary from reading to reading, but this table gives the general idea of the charges that should be observed.

Table 1. Zeta potential values and standard deviations for MUA, PEI, PSS, Lysozyme, and RNA individually.

Compound	Zeta Potential (mV)
MUA	$-22.71 \pm 4.36$
PEI	$21.40 \pm 1.81$
PSS	$-53.12 \pm 2.18$
Lys	$10.74 \pm 1.78$
RNA	$-19.10 \pm 4.21$

The first sample measured was the ZnO-MUA-Lys-PSS-PEI nanoparticle conjugates. Figure 25 shows the average of four zeta potential measurements for the sample. The first measurement for the synthesized zinc oxide particles with MUA in the solution had a zeta potential of -20 mV. Since MUA has a negative charge at physiological pH, there results were

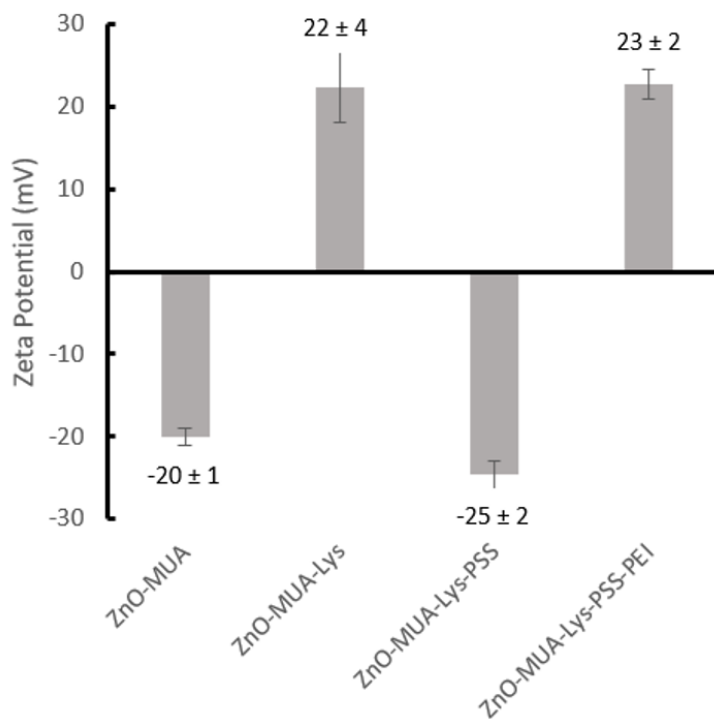


Figure 25. Zeta potential measurements for the ZnO-MUA-Lys-PSS-PEI layered nanoparticle samples after each deposition with mean and standard deviation labelled.

expected. Further layers had the proper charges switching off being positive and negative with +22 mV for lysozyme, -25 mV for PSS, and ending with +23 mV for the layer of PEI on the outside. These results show that the deposition process was successfully completed for each layer and have similar values to the literature values. They do vary however due to the concentrations of the compounds being different.

The sample with zinc oxide attached directly to lysozyme without any stabilizing agent also had the zeta potential measured after each deposition. This sample had the order of layering as ZnO-Lys-PSS-PEI. Figure 26 shows this for the average of four trials after each layer was added. The zinc oxide nanoparticles without anything bound to them had an average of +4 mV for the surface charge. The next layer, lysozyme, also has a positive charge which is why this

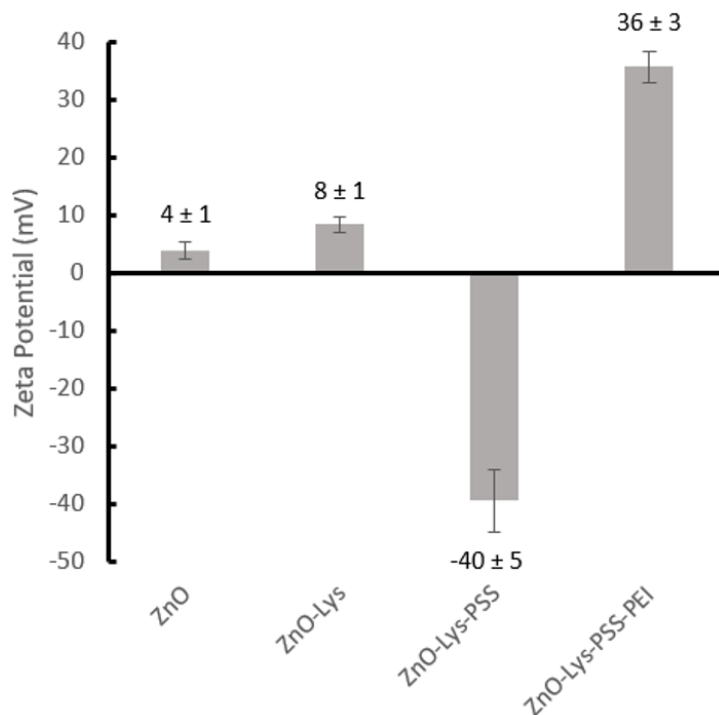


Figure 26. Zeta potential measurements for the ZnO-Lys-PSS-PEI layered nanoparticle samples after each deposition with mean and standard deviation labelled.

binding process took much longer than the other ones (i.e. 24 hours vs. 1 hour). After incubation, the ZnO-Lys sample was measured to have a surface charge of +8 mV. This ideally should have

been higher due to lysozyme being a very positive enzyme at physiological pH. Continuing the layering process, PSS was bound for a charge of -40 mV and finally PEI with a charge of +36 mV as expected. Again, this shows that the deposition process for this sample was successful for the encapsulation of lysozyme in the nanoparticle conjugate since each deposition had the charge switching between positive and negative. The lysozyme binding directly to the zinc oxide nanoparticles worked, but not to the extent that was hoped. The zeta potential measured for ZnO-Lys was lower than expected, which is most likely due to the binding method and that it's a positive to positive interaction. Therefore, although this method did work, the RNA nanoparticle conjugate will use the stabilizing agent of MUA in the deposition process to assure the binding of each layer is through strong electrostatic interactions.

These zeta potential values for each nanoparticle conjugate as well as the known electrostatic interactions between each layer were another method for confirming the successful deposition of each layer and the overall encapsulation of lysozyme. With the results given so far, the deposition process has been shown to work using each characterization technique.

**Section 3.1.5 Fourier-Transform Infrared Spectroscopy.** In addition to the other characterization techniques completed, IR spectroscopy was also used to confirm the presence of MUA and the encapsulated species within the nanoparticle conjugate. When looking at the known spectra for these materials, MUA should have peaks at about  $2900\text{ cm}^{-1}$ ,  $2600\text{ cm}^{-1}$ , and  $1680\text{ cm}^{-1}$ . These represent the saturated alkyls, the sulfur, and the carboxylic acid respectively in the MUA chain.<sup>49</sup> Lastly, lysozyme can be characterized by its two known amide peaks around  $1650\text{ cm}^{-1}$  for Amide I and  $1540\text{ cm}^{-1}$  for Amide II.<sup>16</sup> With these known values, the IR spectra for the nanoparticle conjugate samples were analyzed. When analyzing these samples, it was found that the PEI and PSS layers did not have any effect on the spectra obtained, so

therefore were not included in this data. The purpose of this section was to see that lysozyme was present in the sample by observing the amide peaks.

The first nanoparticle conjugate looked at was with lysozyme bound directly to the zinc oxide nanoparticle. Figure 27 shows this sample before and after the deposition of the lysozyme layer to compare and confirm the presence of the enzyme. The spectra for the original zinc oxide sample and for the lysozyme layered sample, ZnO-Lys, were graphed together to be able to

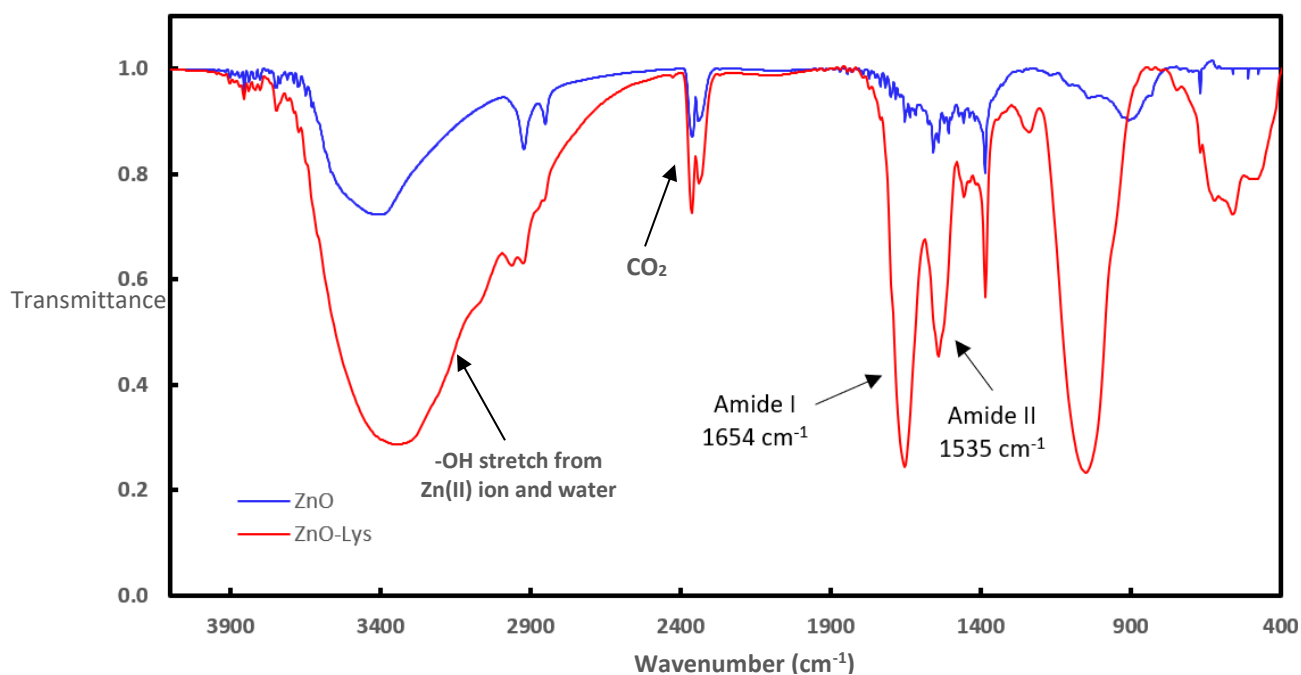


Figure 27. FTIR Spectra for ZnO-Lys-PSS-PEI samples before and after the deposition of lysozyme with the amide peaks labelled.

compare peaks easily. The main peaks to notice are the two amide peaks labelled at 1650 and 1530 cm<sup>-1</sup> for ZnO-Lys in correlation with the literature peaks.<sup>16</sup> The other peaks, some labelled, were not important to this analysis technique. The two amide peaks correlate to the amides in the amino acids of lysozymes sequence. The presence of these peaks show that lysozyme was in fact bound to the zinc oxide in this sample. Looking at the ZnO sample, there are no amide peaks seen which was expected due to no lysozyme being present in that sample. Moreover, these

spectra show the presence of lysozyme in this nanoparticle conjugate sample. These results along with others confirm the deposition of lysozyme.

The other sample characterized with IR spectroscopy was ZnO-MUA-Lys-PSS-PEI. Specifically, the spectra measured were for the starting material of ZnO-MUA and the first deposition of lysozyme and are shown in Figure 28. The first was for the original nanoparticle conjugates, ZnO-MUA. Looking at the spectra, the blue spectrum has peaks corresponding to the

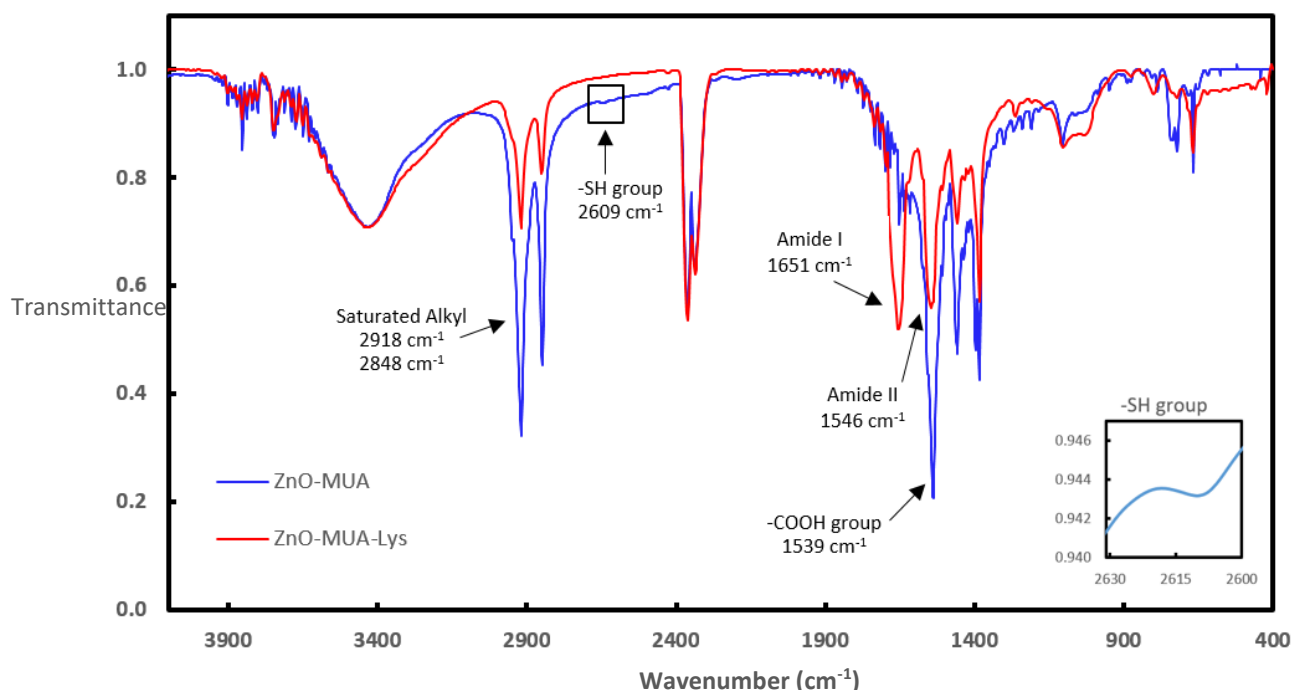


Figure 28. FTIR Spectra for ZnO-MUA-Lys-PSS-PEI samples before and after the deposition of RNA with the amide peaks labelled.

functional groups of MUA in accordance with the literature which are labelled.<sup>49</sup> To see that the -SH peak was actually present, a zoomed in image is in the bottom right corner of the figure.

Further analysis with the ZnO-MUA-Lys sample showed the amide peaks where they were expected to be seen at 1650 and 1540 cm<sup>-1</sup>. These peaks are less intense than literature spectra show, but was expected due to the high concentration of MUA in this sample. Overall, MUA and

lysozyme were shown to bind to the nanoparticle conjugate as hoped for. Again, these results show that lysozyme was successfully bound and encapsulated into the vessel.

These spectra were in accordance with the UV-Vis spectra shown previous sections showing the presence of lysozyme in each sample. Peaks were visible in each type of spectrum accounting for the species on the outside of the conjugate. With all the characterization analyses completed thus far, it can be concluded that the deposition process for each of these nanoparticle conjugates were completed successfully for the encapsulation of lysozyme. Next, the integrity of each material must be tested to assure that it will still be active and, therefore, useful once transported through a cell membrane.

**Section 3.1.6 Activity of Lysozyme.** The last experiment to characterize the synthesized zinc oxide nanoparticles encapsulating lysozyme was a lysozyme activity assay using the UV-Vis spectrophotometer. This was done to verify the activity of lysozyme within the layered particles. The enzymatic activities for free lysozyme and for the encapsulated lysozyme within the zinc oxide nanoparticles were monitored for 30 minutes within the UV-Vis spectrophotometer. The bacteria sample was added to the bioconjugate sample to see how the surface interaction between them evolved. Figure 29 shows the enzymatic activities of each sample over time. After 5 minutes, the activity of free lysozyme greatly decreased and reached zero after 15 minutes. This shows that after this amount of time, the native lysozyme had fully digested the bacteria in the assay. Then, when looking at both encapsulated lysozyme samples, the activity had a much different behavior due to the particles being layered causing the lysozyme not to be released into the bacteria immediately. Overall, the enzymatic activity increased in the first 10 minutes for each sample due to the polymeric layers on the outside of the conjugate. After 10 minutes, the ZnO-MUA-Lys-PSS-PEI conjugates began to decrease in

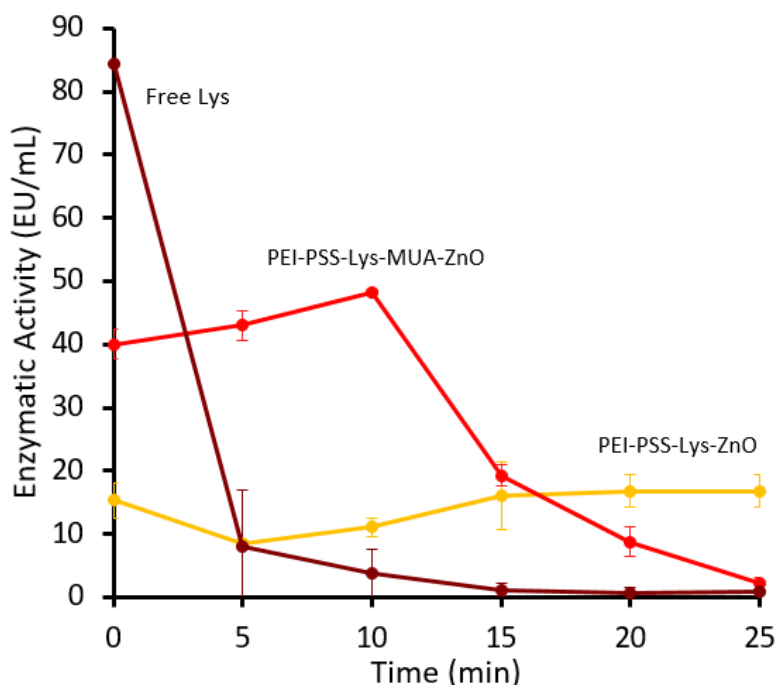


Figure 29. Lysozyme activity assay for a free lysozyme sample and the two layered samples when added to a solution of bacteria measured in  $\text{EU/mL}_{\text{enzyme sample}}$ . (error bars on all data points, some not visible due to precision)

enzymatic activity reaching nearly zero at 25 minutes. On the other hand, the ZnO-Lys-PSS-PEI conjugates continued to have an increase in the enzymatic activity after 10 minutes reaching a plateau by 25 minutes. Zinc oxide has a high affinity for enzymes which may have prolonged the activity of the lysozyme once in the bacteria.

These results for the samples encapsulating lysozyme show that the nanoparticle conjugate could be transported into a cell before the lysozyme would be released. The vessel would penetrate the cell membrane before diffusion of the enzyme would take place due to the outside layers of PSS and PEI needing to be removed first. Therefore, these results show that lysozyme was still active inside the nanoparticle conjugates after a certain time. Furthermore, these results match the gold nanoparticle conjugate results very well with the activity increasing for both layered samples in that case, too. With these results in accordance with each other, the lysozyme



encapsulation process can be concluded to work for its transport into cells via a nanoparticle delivery system.

### Section 3.2 Encapsulation of RNA

After completed the first goal of synthesizing a delivery system using zinc oxide nanoparticles, the model protein encapsulated was replaced with a more useful drug. The results here show how RNA was successfully encapsulated within the nanoparticle conjugate for transport into cells. The layering was ordered as follows: ZnO-MUA-PEI-RNA-PEI.

**Section 3.2.1 UV-Vis Spectrophotometry.** The last nanoparticle conjugates made in this experiment were synthesized to encapsulate RNA instead of lysozyme. The ordering of layers changed due to the PSS being unnecessary, so it was not seen in the spectra at all. For the ZnO-MUA-PEI-RNA-PEI sample, the absorbance spectra were obtained from 200 to 800 nm with 1 mM NaCl being used for the blank as before. Figure 30 shows the absorbance spectrum after

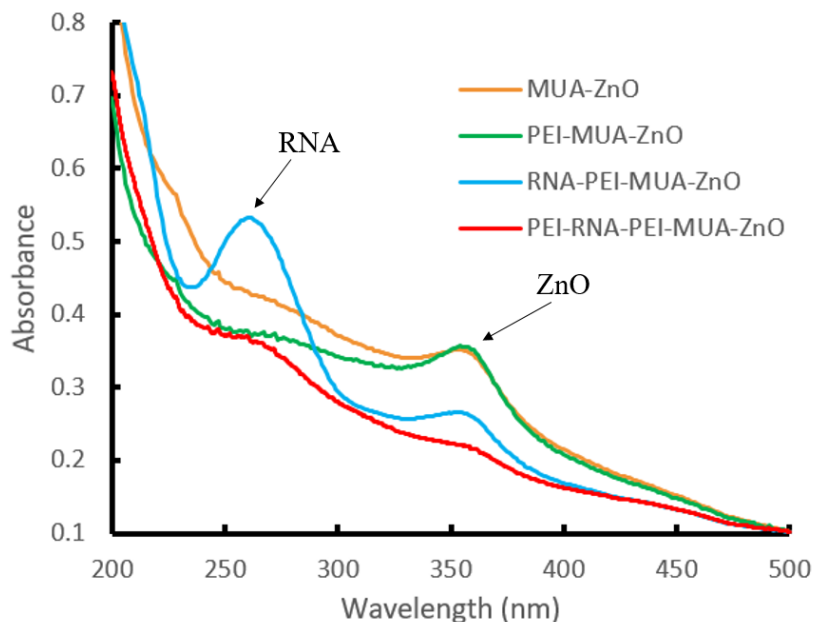


Figure 30. Absorbance Spectra for ZnO-MUA-PEI-RNA-PEI layered nanoparticle samples after each deposition.

each deposition for this process. The zinc oxide concentration was increased for these particles, while the MUA concentration was decreased (see experimental section for exact concentrations), making the characteristic zinc oxide peak at 360 nm present in each spectrum throughout the layering process. Specifically, the zinc oxide peak was seen as expected in each spectrum at 360 nm, although the intensity was much lower in the final product due to the high concentration of PEI on the outside. When RNA was the outer-most layer, its characteristic peak was seen very well at 260 nm showing the successful deposition of RNA to the conjugate. However, once PEI was layered on top of it, the peak intensity decreased immensely, which was similar to the zinc oxide peak, but can still be observed at 260 nm. Overall, the presence of RNA and zinc oxide were confirmed with these spectra meaning that these preliminary results show that this method is effective.

**Section 3.2.2 Scanning Electron Microscopy.** As before, the SEM was used to analyze the nanoparticles encapsulating RNA before and after deposition. For the ZnO-MUA-PEI-RNA-PEI NP sample, these nanoparticles were synthesized with slightly different parameters than the ones discussed earlier (See experimental section for specific conditions). The deposition process was looked at before anything was added to the particles and after all the layering was completed. Figure 31 (A) shows the nanoparticle conjugates of ZnO-MUA before any layering occurred. With the new synthesis process, these particles were observed to have a needle shape to begin with their length averaging around 250 nm with a much smaller diameter meaning they were still nano-sized as expected. Figure 31 (B) then shows the nanoparticle conjugates after the entire deposition process was completed. These particles have an ordering of layers as ZnO-MUA-PEI-RNA-PEI. Again, these nanoparticle conjugates have a needle-like shape and were

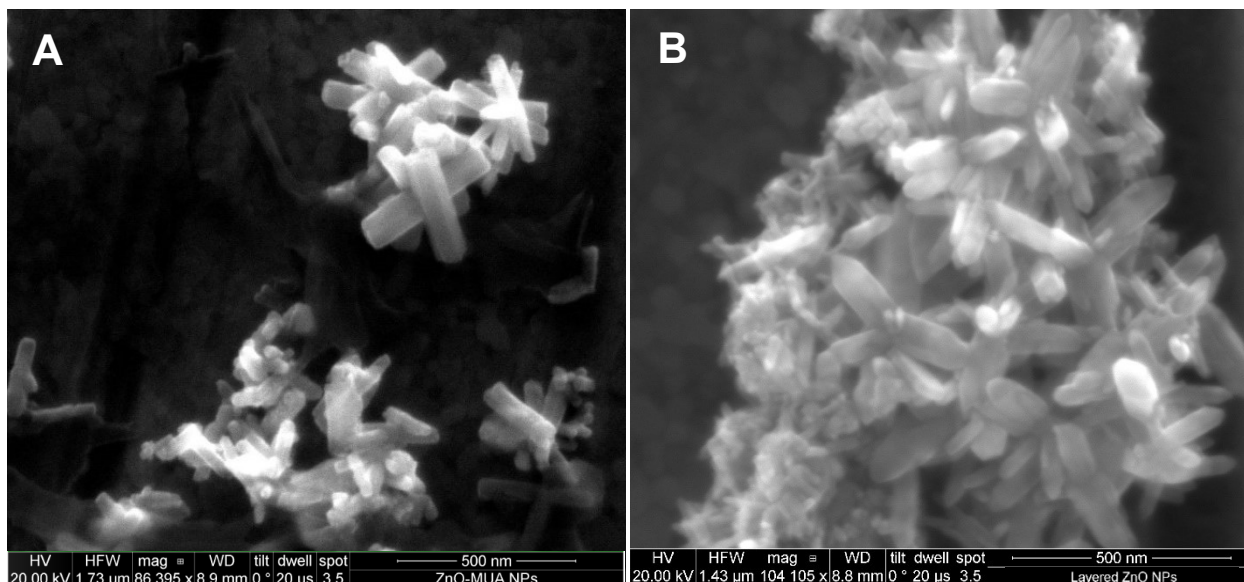


Figure 31. SEM images taken for the ZnO-MUA-PEI-RNA-PEI NP samples (A) before and (B) after deposition with the scale bar in the right corner of each to estimate the size of the particles.

more aggregated after the deposition process. However, their size did increase to have a thicker diameter and longer length of about 500 nm as expected. These results were not exactly what was expected with the shape of the particles, although the parameters could easily be changed in the original synthesis process to make the nanoparticles more spherical than needle-like. To do this, the temperature the particles were synthesized at would need to be increased. The MUA in the synthesis process was hypothesized to change the exact parameters needed for spheres to form.

**Section 3.2.3 Dynamic Light Scattering.** The nanoparticle conjugates encapsulating RNA with a final ordering of ZnO-MUA-PEI-RNA-PEI were further analyzed with the DLS for diameter and polydispersity measurements. These were measured after each deposition and are shown in Figure 32 for an average of four trials. The starting material of ZnO-MUA was measured at 250 nm. As each following layer was added, the nanoparticle conjugate increased in size as expected with the PEI layer being 290 nm, RNA at 397 nm, and the final product at 488

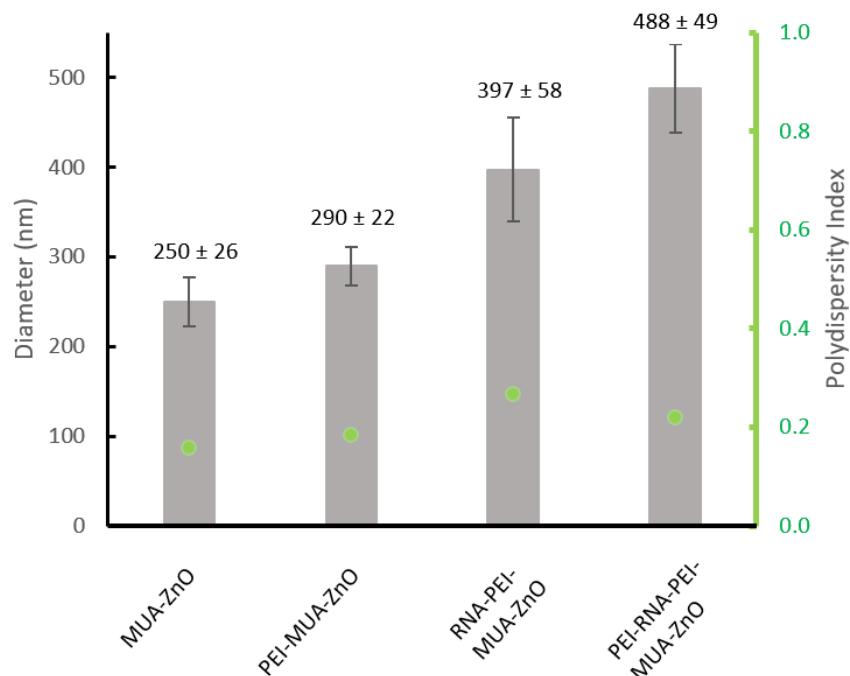


Figure 32. Particle diameter (left axis) and polydispersity (right axis) of ZnO-MUA-PEI-RNA-PEI conjugates measured with the DLS with mean and standard deviation labelled.

nm with the outside layer of PEI. Although these particles are larger than the other samples synthesized with lysozyme instead of RNA, the deposition process still worked well and showed a preliminary conclusion that RNA was encapsulated successfully. These results also matched well with the SEM measurements to within 20 nm.

**Section 3.2.4 Zeta Potential.** As previously discussed, the RNA nanoparticle conjugate sample has a layering of ZnO-MUA-PEI-RNA-PEI to have electrostatic interactions between each layer. These samples had the zeta potential measured after each layer to assure the encapsulation of RNA. Figure 33 shows the charge after each layer for this sample averaging four trials. The beginning sample of ZnO-MUA started with a charge of -25 mV. From there, it increased to +31 mV with PEI, decreased to -17 mV with RNA, and back to +26 mV with the last layer of PEI. The RNA had a negative zeta potential value as expected showing the successful deposition of that layer to the nanoparticle conjugate. Overall, this sample had each

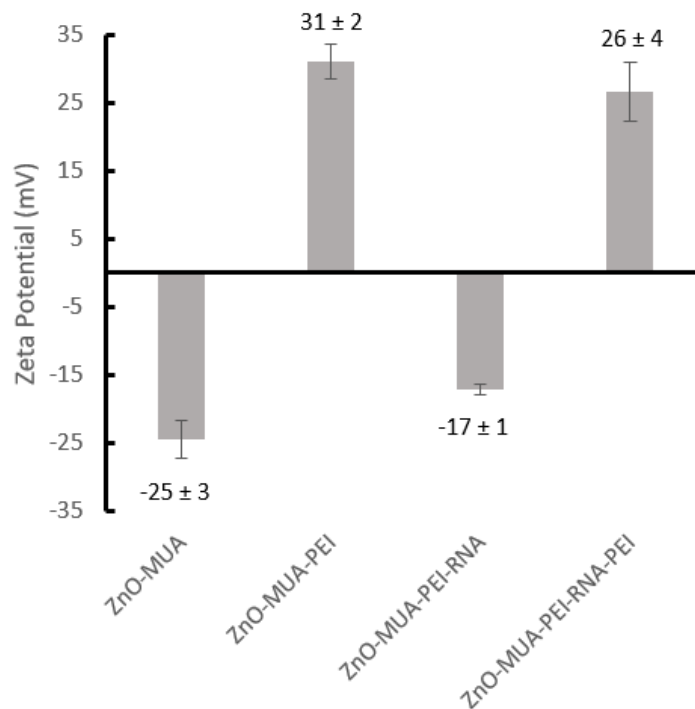


Figure 33. Zeta potential measurements for the ZnO-MUA-PEI-RNA-PEI layered nanoparticle samples after each deposition with mean and standard deviation labelled.

layer bound as expected to the conjugate with high zeta potential values representing high concentrations.

**Section 3.2.5 Fourier-Transform Infrared Spectroscopy.** Looking at RNA, its FTIR spectrum depends specifically on the sequence of the RNA used. Generally, according to literature, it should have peaks in the range of  $1700$  to  $1400\text{ cm}^{-1}$  showing the G, A, C, and U bases in the sequence. In addition, it will have a peak around  $1220\text{ cm}^{-1}$  for the  $\text{PO}_2$ - ribose asymmetric stretch.<sup>50</sup> The nanoparticle conjugate with RNA encapsulated inside had two FTIR spectra obtained for it. The first was for the original nanoparticle conjugates, ZnO-MUA. Looking at the spectra shown in Figure 34, the blue spectrum shows the functional groups of MUA in accordance with the literature with the peaks labelled.<sup>49</sup> To see the -SH peak was present, a zoomed in image is in the bottom right corner. The second spectrum shown for this

particular sample was after the deposition of RNA with the ordering of ZnO-MUA-PEI-RNA. Although the literature peaks for RNA are very general, specific ones can be seen from 1650 to 1450  $\text{cm}^{-1}$  representing the G, A, C, and U bases present in the sequence.<sup>50</sup> Furthermore, the  $\text{PO}_2^-$  bonded to the ribose is seen at 1222  $\text{cm}^{-1}$  as expected. Overall, this shows the successful

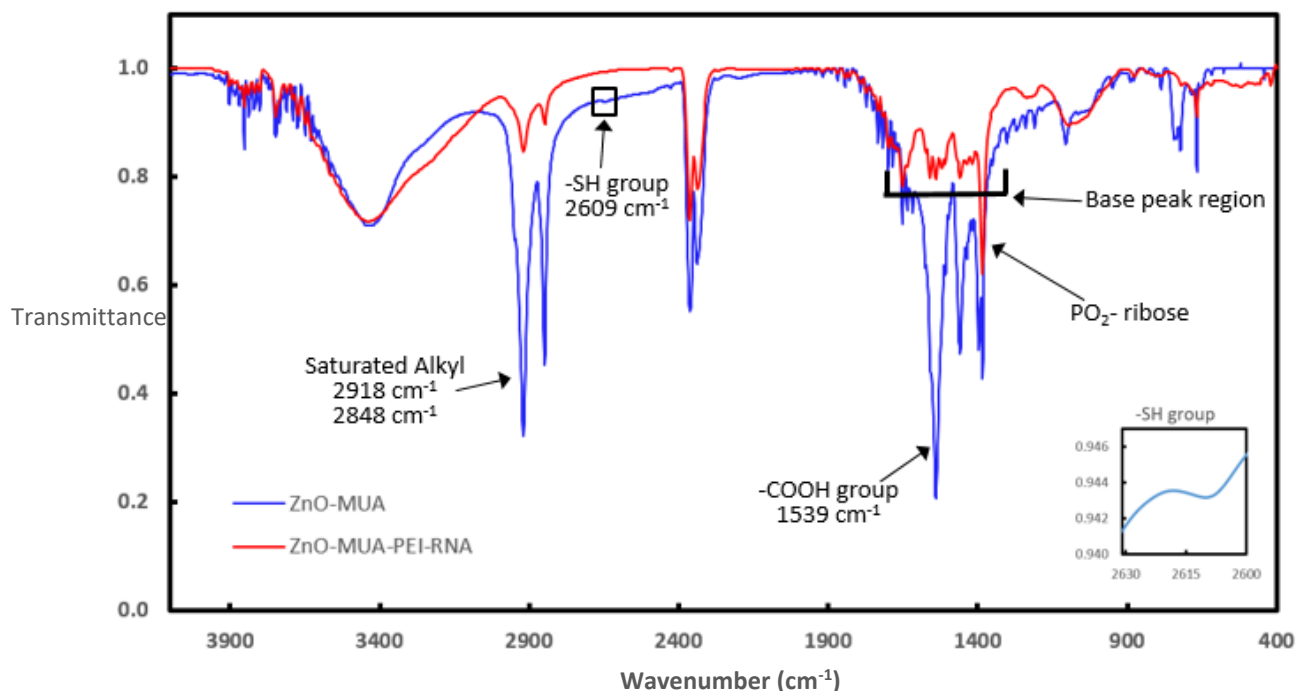


Figure 34. FTIR Spectra for ZnO-MUA-PEI-RNA-PEI samples before and after the deposition of RNA with the important peaks labelled for MUA.

deposition of MUA in the original sample and of RNA in the final sample. Due to RNA not having a designated literature IR spectrum, this is not the best way to confirm the presence of nucleic acids in the nanoparticle samples.

**Section 3.2.6 Integrity of RNA.** The integrity of the encapsulated RNA was determined using fluorescence spectroscopy with an ethidium bromide assay. To assure that this process would work efficiently and to have a standard to compare the experimental sample to, free RNA was bound to ethidium bromide, degraded, and analyzed as a reference. The RNA degradation

was completed using two different methods as stated in the experimental section. The first one to be looked at was the degradation with acid. Figure 35 shows these results for three samples with various conditions. Ethidium bromide by itself was measured to assure it had very little to no fluorescence without intercalating into RNA. In addition, RNA was tested by itself and had the least fluorescence of all the samples. Next, RNA and ethidium bromide were added together which caused the ethidium bromide to act as a fluorescent tag on the RNA. The fluorescence then greatly increased as seen on the graph. However, with degradation of the RNA using an

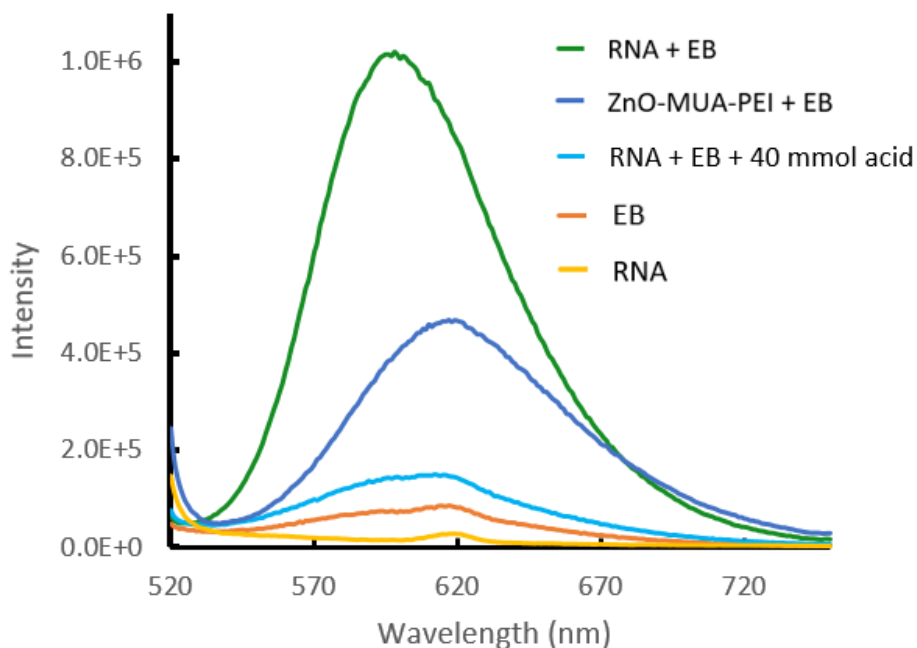


Figure 35. Standard RNA integrity assay using ethidium bromide and fluorescence spectroscopy for three samples: EB- ethidium bromide, RNA bound to ethidium bromide, and RNA bound to ethidium bromide with HCl added to degrade the sample.

acid, in this case hydrochloric acid, the fluorescence of the sample decreased to be almost equal with the ethidium bromide sample by itself. This is due to the RNA being degraded to the point that it is unusable. For this sample of RNA, it took 40 mmol of 0.1 M HCl to degrade the sample to that low of an intensity. After the addition of only one drop, the fluorescence began to decrease and continued with the addition of more acid, as expected. Finally, to assure that the

bioconjugate would fluoresce due to the RNA and not the PEI, the bioconjugates with layers ZnO-MUA-PEI were mixed with ethidium bromide. These are shown to be fluorescent but not to the degree that RNA is with the intercalating agent.

For the next degradation technique, the standard RNA sample was degraded by heating in a water bath. An RNA sample without any heating was measured for fluorescence along with the heated sample. Figure 36 shows these results for both samples with ethidium bromide intercalated into them. The sample with no degradation had a large peak at 600 nm as expected to show the high fluorescence of ethidium bromide when bound to intact RNA. On the other

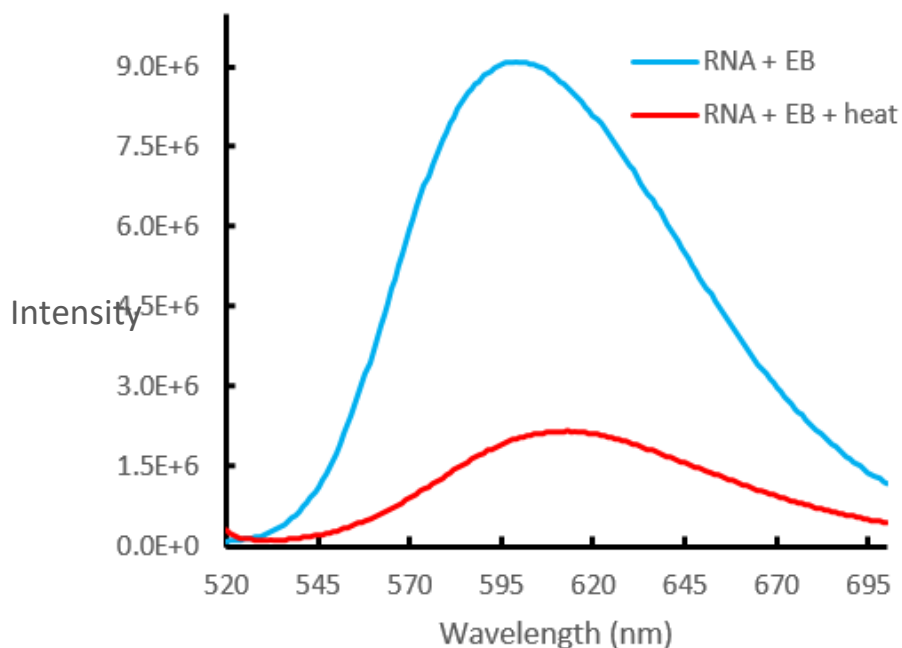


Figure 36. Standard RNA integrity assay using ethidium bromide and fluorescence spectroscopy for two samples: RNA bound to ethidium bromide, and RNA bound to ethidium bromide heated at 120°C.

hand, the heated sample had a much lower fluorescence as seen on the graph. The peak is much shallower than the non-heated sample, meaning that the sample in question was successfully degraded to a point. However, the fluorescence of this degraded RNA sample is still much higher than the one degraded by acid seen in Figure 35. Overall though, both degradation techniques



worked and showed that intact RNA will have a much higher fluorescence than degraded RNA. This means that this test will work well for determining if the encapsulated RNA sample is degraded or intact and can therefore be effective in gene regulation once transported into cells.

From there, the integrity of the encapsulated RNA was tested using the same methods as for the standard RNA. First off, the encapsulated RNA sample was added to ethidium bromide and measured for fluorescence. Figure 37 shows this trial with a large peak at about 610 nm. At this point, comparing this sample to the one with only ethidium bromide, it can be assumed that

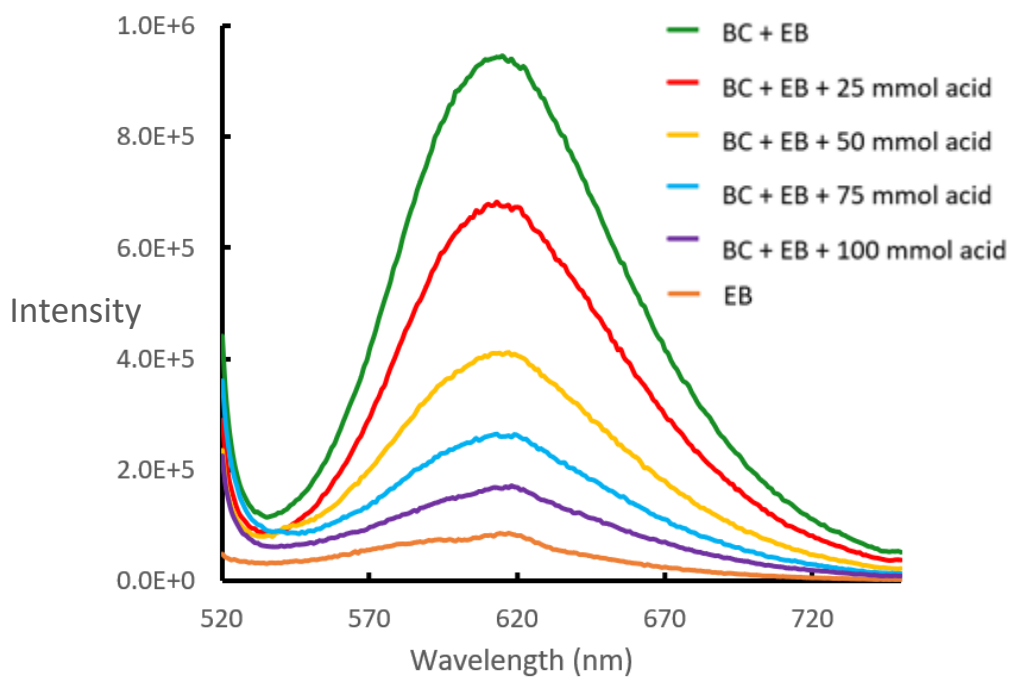


Figure 37. RNA integrity assay for the nanoparticle bioconjugates encapsulating RNA using ethidium bromide and fluorescence spectroscopy: EB- ethidium bromide, bioconjugates bound to ethidium bromide, and bioconjugates bound to ethidium bromide with various amounts of HCl added to degrade the sample (shows total amount added).

the RNA is intact. However, to assure that it is, multiple trials were completed with adding different amounts of acid to this sample to see how the fluorescence was affected. Figure 36 shows the fluorescence spectra for the nanoparticle conjugates encapsulating RNA bound to

ethidium bromide with acid added ranging from 25 to 100 mmol. As seen in the graph, the fluorescence slowly decreased as the amount of acid increased showing that the RNA was being degraded as more acid was added. More acid was needed to degrade the encapsulated RNA than the free RNA sample due to layers of polyelectrolytes protecting it from the acid in the sample. Those layers had to be removed by reacting with the acid first before the RNA could be fully released for degradation.

Next, the second method for degradation was completed for the encapsulated RNA sample. This degradation method involved heating the encapsulated RNA sample in 120°C water bath for 10 minutes to start with. Figure 38 shows the original nanoparticle conjugates bound with ethidium bromide. This sample had a very high fluorescence as expected, shown by the peak at about 610 nm. The sample was then attempted to be degraded by heating it for 10 minutes. However, this had minimal change to the fluorescence of the sample, so heating was

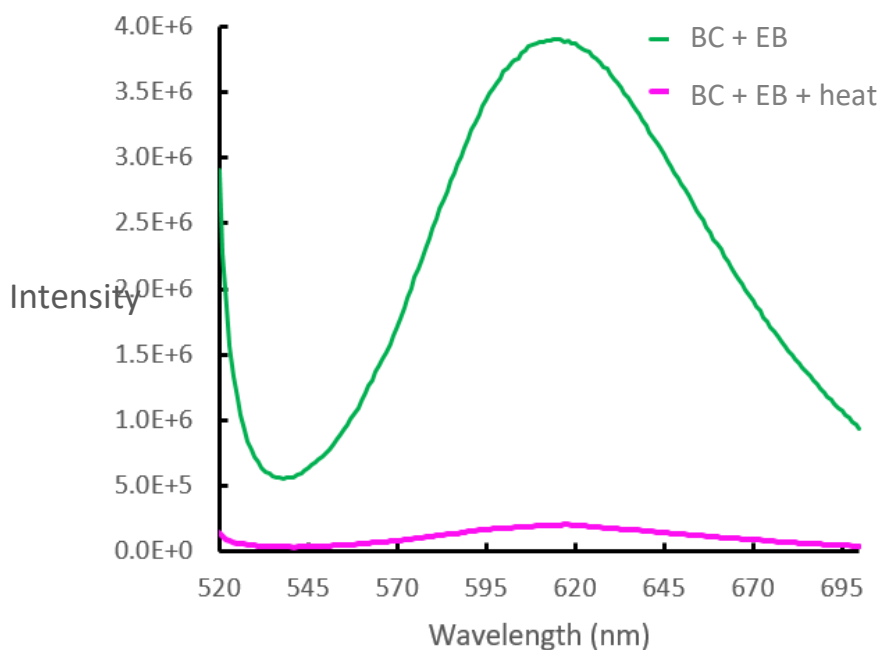


Figure 38. RNA integrity assay for the nanoparticle bioconjugates encapsulating RNA using ethidium bromide and fluorescence spectroscopy: bioconjugates bound to ethidium bromide, and bioconjugates bound to ethidium bromide heated at 120°C.

continued for 30 minutes to assure degradation would take place. After this time in the hot water bath, the sample had a very low fluorescence as seen in Figure 37. This degradation process took much longer than expected, however, according to the literature. With the RNA being encapsulated though, again the polyelectrolyte layers would have to be removed before the RNA could be degraded within the sample. Therefore, these results do show the proper degradation of the sample after heating for 30 minutes.

Overall, both ethidium bromide assays for the encapsulated RNA samples show that the RNA is in fact intact and useable for gene silencing or regulation once transported into cells. They also show that the layering process worked well in protecting the RNA from its surroundings for a time which will allow the nanoparticle conjugate to penetrate the cell wall before releasing the RNA. However, the acid degradation results are more conclusive since no parameters were changed from one test to the next. The heating method had to be extended for heating time compared to literature protocols.

## CHAPTER 4. CONCLUSION

Through this research, it was shown that zinc oxide nanoparticles were synthesized with different modifications to the particles. With near ambient conditions and no activators needed, these nanoparticle conjugates were easily produced and characterized using zinc chloride and sodium hydroxide. Three different layering techniques were used, two of which encapsulated lysozyme, and the other encapsulated RNA. The general basis for encapsulation started with the zinc oxide nanoparticle core, MUA added for stabilization in some cases, and then polyelectrolytes and the biological material in question layered after that depending on the charge of each. The final products were as follows: ZnO-MUA-Lys-PSS-PEI, ZnO-Lys-PSS-PEI, and ZnO-MUA-PEI-RNA-PEI.

After each layering step, the diameter, surface charge, FTIR spectrum, and UV-Vis spectrum were looked at to determine if each deposition was successfully layered. The optical properties and zeta potential measurements concluded the presence of each layer on to the conjugate. The diameter measurements showed that the nanoparticles increased in size with each deposition ending with various diameters for each sample averaging 300 nm. Furthermore, the images from the SEM allowed observation of the particle size and shape before and after the deposition process. None of the three nanoparticle samples had a uniform shape across the film when observed. Ideally, the particles would have been spherical which further research could possibly fix with increased reaction temperature.

The last characterization techniques completed for the nanoparticle conjugates were the assays to assure the effectiveness of the biological materials, lysozyme and RNA, once transported into the cells. These tests had promising results showing that the encapsulated

material was still active and intact, and that the outside polyelectrolyte layers successfully protected the material for a time. This will allow for the biological material to be transported into the cell before the outside layers are removed. Once in the cell and the layers have come off, the RNA or lysozyme can diffuse into the cell for its biological purpose.

All three nanoparticle conjugates were synthesized with each layer being confirmed, however, each had particular aspects that worked better due to the particular synthetic process used. The nanoparticle conjugate encapsulating RNA had the most conclusive results overall. All layers were seen to bind properly through UV-Vis spectroscopy as well as zeta potential measurements. Furthermore, the diameter of the particles steadily increased with each layering by about 30 nm. The only adjustment to be made with these particles are their shape. The SEM images show long needle-like shapes instead of spheres. Increasing the reaction temperature would most likely fix this issue according to past research.<sup>27</sup> In brief, the ZnO-MUA-PEI-RNA-PEI nanoparticle sample worked the best in these synthesis processes.

As for the lysozyme encapsulated samples, these had various unexpected results. These issues were fixed when redone for the nanoparticle conjugate encapsulating RNA instead of lysozyme. Specifically, the sample with MUA in it did not have a high enough concentration of zinc oxide in the sample to begin with. It also did not have a steady increase in diameter as expected. For the ZnO-Lys-PSS-PEI sample, the zeta potential for lysozyme was not as high as was hoped, and furthermore, not enough lysozyme was bound into the system.

Overall, the zinc oxide nanoparticle conjugates were synthesized and analyzed successfully with a few improvements that can be made in the future. Furthermore, the conjugates showed promising results for the transfection of the proteins into cells. From here, these nanoparticle conjugates could be tested in the actual transport into cells using past methods

in the literature. This would show firsthand that these conjugates would work in the transport of biological material into cells. However, this research has given a general basis to start with and shown that these nanoparticle conjugates will work as a delivery system as expected.

## REFERENCES

- (1) “Nanotechnology Timeline.” *Nanotechnology 101*. National Nanotechnology Initiative **2014**. <https://www.nano.gov/timeline>.
- (2) Khan, I; Saeed, K; Khan, I. Nanoparticles: Properties, Applications, and Toxicities. *Arabian Journal of Chemistry* **2017**.
- (3) “Nanomaterials.” National Institute of Environmental Health Sciences **2018**. <https://www.niehs.nih.gov/health/topics/agents/sya-nano/index.cfm>.
- (4) Salata, O. V. Applications of Nanoparticles in Biology and Medicine. *Journal of Nanobiotechnology* **2004**, *2*, 1-6.
- (5) “What’s So Special about the Nanoscale?” *Nanotechnology 101*. National Nanotechnology Initiative **2003**. <https://www.nano.gov/nanotech-101/special>.
- (6) Rao, C.N.R.; Muller, A.; Cheetham, A.K.: The Chemistry of Nanomaterials: Synthesis, Properties and Applications. *Wiley-VCH* **2004**.
- (7) “Nanomaterials.” *Hawk’s Perch Technical Writing*. Understanding Nano **2007**. <http://www.understandingnano.com/nanomaterials.html>.
- (8) Gann, H.; Glaspell, G.; Garrad, R.; Wanekaya, A.; Ghosh, K.; Cillessen, L.; Scholz, A.; Parker, B.; Warner, M.; Delong, R. K. Interaction of MnO and ZnO Nanomaterials with Biomedically Important Proteins and Cells. *J. Biomed. Nanotechnol.* **2010**, *6* (1), 37–42.
- (9) Barber, S.; Abdelhakiem, M.; Ghosh, K.; Mitchell, L.; Spidle, R.; Jacobs, B.; Washington, L.; Li, J.; Wanekaya, A.; Glaspell, G.; et al. Effects of Nanomaterials on Luciferase with Significant Protection and Increased Enzyme Activity Observed for Zinc Oxide Nanomaterials. *J. Nanosci. Nanotechnol.* **2011**, *11* (12), 10309–10319.
- (10) Hobbs, J. M.; Patel, N. N.; Kim, D. W.; Rugutt, J. K.; Wanekaya, A. K. Glucose Determination in Beverages Using Carbon Nanotube Modified Biosensor: An Experiment for the Undergraduate Laboratory. *J. Chem. Educ.* **2013**, *90* (9), 1222–1226.
- (11) Foster, S.; Duvall, C. L.; Crownover, E. F.; Hoffman, A. S.; Stayton, P. S. Intracellular Delivery of a Protein Antigen with an Endosomal-Releasing Polymer Enhances CD8 T-Cell Production and Prophylactic Vaccine Efficacy. *Bioconjug. Chem.* **2010**, *21* (12), 2205–2212.
- (12) Wurster, E.-C.; Elbakry, A.; Göpferich, A.; Breunig, M. Layer-by-Layer Assembled Gold Nanoparticles for the Delivery of Nucleic Acids. *Methods Mol. Biol.* **2013**, *948*, 171–182.
- (13) “Electrostatic Interaction.” Illustrated Glossary of Organic Chemistry. *Chem.UCLA*. [http://www.chem.ucla.edu/~harding/IGOC/E/electrostatic\\_interaction.html](http://www.chem.ucla.edu/~harding/IGOC/E/electrostatic_interaction.html).
- (14) Baker, Z.; Saltik, M.; Lehrmann, H.; Killisch, I.; Mautner, V.; Lamm, G.; Christofori, G.; Cotton, M. Polyethylenimine (PEI) is a Simple, Inexpensive and effective Reagent for Condensing and Linking Plasmid DNA to Adenovirus for Gene Delivery. *Gene Therapy* **1997**, *4*, 773-782.
- (15) Kaczmarek, J. C.; Kowalski, P. S.; Anderson, D. G. Advances in the Delivery of RNA Therapeutics: From Concept to Clinical Reality. *Genome Medicine* **2017**, *9* (60), 1-16.

- (16) Garcia-Hernandez, C.; Freese, A.; Rodriguez-Mendez, M. L.; Wanekaya, A. K. In Situ Synthesis, Stabilization and Activity of Protein Modified Gold Nanoparticles for biological Applications. *Biomaterials Science* **2019**, 1-9.
- (17) DeLong, R. K.; Reynolds, C. M.; Malcolm, Y.; Schaeffer, A.; Severs, R.; Wanekaya, A. Functionalized Gold Nanoparticles for the Binding Stabilization, and Delivery of Therapeutic DNA, RNA, and other biological Macromolecules. *Nanotechnology, Science and Applications* **2010**, 3, 53-63.
- (18) “Dynamic Light Scattering Technology.” *Horiba*. <http://www.horiba.com/scientific/products/particlecharacterization/technology/dynamic-light-scattering/>
- (19) “Zeta potential: Layout, Calculation, Analysis.” *Horiba*. <http://www.horiba.com/en-en/zeta-potential/>
- (20) “Determining the Isoelectric Point (IEP) in Engineered Particles.” AZoMaterials. **2014**. <https://www.azom.com/article.aspx?ArticleID=11523>
- (21) Kumar, S. S.; Venkateswarlu, P.; Rao, V. R.; Rao, G. N. Synthesis, Characterization and Optical Properties of Zinc Oxide Nanoparticles. *International Nano Letter* **2013**, 3, 30.
- (22) “Zinc Oxide.” *Molecule of the Week Archive*. American Chemical Society **2014**. <https://www.acs.org/content/acs/en/molecule-of-the-week/archive/z/zinc-oxide.html>
- (23) Wang, Z. L. Zinc Oxide Nanostructures: Growth, Properties and Applications. *Journal of Physics: Condens. Matter* **2004**, 16, 829-858.
- (24) Coonis, T.; Wanekaya, A.; Simpson, A.; Duszynski, M. Electrodeposition of Metal Oxides Using Deep Eutectic Solvents. *Missouri State University*. **2015**.
- (25) Mishra, P. K.; Mishra, H.; Ekielski, A.; Talegaonkar, S.; Vaidya, B. Zinc Oxide Nanoparticles: A Promising Nanomaterial for Biomedical Applications. *Drug Discovery Today* **2017**, 22 (12), 1825-1834.
- (26) Schwartz, V. B.; Thetiot, F.; Ritz, S.; Putz, S.; Choritz, L.; Lappas, A.; Forch, R.; Landfester, K.; Jonas, U. Antibacterial Surface Coatings from Zinc Oxide Nanoparticles Embedded in Poly(N-isopropylacrylamide) Hydrogel Surface Layers. *Adv. Funct. Mater.* **2012**, 22, 2376-2386.
- (27) Spidle, R.; Size-Dependent Synthesis, Characterization and Biomedical Applications of Zinc Oxide Nanoparticles. *MSU Graduate Theses* **2012**, 1988, 1-104.
- (28) Reddy, K. M.; Feris, K.; Bell, J.; Wingett, D. G.; Hanley, C.; Punnoose, A. “Selective Toxicity of Zinc Oxide Nanoparticles to Prokaryotic and Eukaryotic Systems.” *Applied Physics Letters* **2007**, 90 (213902).
- (29) Chakraborti, S.; Chatterjee, T.; Joshi, P.; Poddar, A.; Bhattacharyya, B.; Singh, S. P.; Gupta, V.; Chakarabarti, P. Structure and Activity of Lysozyme on Binding to ZnO Nanoparticles. *Langmuir* **2010**, 26 (5), 3506-3513.
- (30) Ischenko, V.; Polarz, S.; Grote, D.; Stavarache, V.; Fink, K.; Driess, M. Zinc Oxide Nanoparticles with Defects. *Adv. Funct. Mater.* **2005**, 15, 1945-1954.



- (31) Chimanpure, J.; Ashtaputre, S.; Marathe, S.; Hebalkar, N.; Kharrazi, S.; Pasricha, Renu; Kulkarni, S. K. Synthesis and Characterization of Mercaptoethanol Capped Zinc Oxide Nanoparticles Capped with Organic Molecules. *Synthesis and Reactivity in Inorganic, Metal-Organic, and Nano-Metal Chemistry* **2006**, *36* (1), 65–69.
- (32) Oladrian, A. A.; Olabisi, I. Synthesis and Characterization of ZnO Nanoparticles with Zinc Chloride as Zinc Source. *Asian Journal for Natural & Applied Sciences* **2013**, *2* (2), 41-44.
- (33) Jones, F. Piezoelectronic Properties of ZnO and its Potential to Power Nanotech. Van Heuvelen Lab at Harvey Mudd College. <http://blogs.hmc.edu/vanheuvelen/the-elements/>.
- (34) Simsikova, M.; Antalík, M.; Kanuchova, M.; Skvarla, J. Anionic 11-Mercapoundecanoic Acid Capped ZnO Nanoparticles. *Applied Surface Science* **2013**, *282*, 342-347.
- (35) “BMRB Featured System: Lysozyme.” *Biological Magnetic Resonance Data Bank*. Worldwide Protein Data Bank. <http://www.bmrwisc.edu/featuredSys/Lysozyme/>.
- (36) Ganguli, S.; Yoshimoto, K.; Tomita, S.; Sakuma, H.; Matsuoka, T.; Shiraki, K.; Nagasaki, Y. Regulation of Lysozyme Activity Based on Thermotolerant Protein/Smart Polymer Complex Formation. *J. Am. Chem. Soc.* **2009**, *131*, 6549-6553.
- (37) Ding, Y.; Shi, L.; Wei, H. Protein-Directed Approaches to Functional Nanomaterials: A Case Study of Lysozyme. *J. Mater. Chem.* **2014**, *2* (47), 8268–8291.
- (38) Zhang, T.; Zhou, P.; Zhan, Y.; Shi, X.; Lin, J.; Du, Y.; Li, X.; Deng, H. Pectin/lysozyme Bilayers Layer-by-Layer Deposited Cellulose Nanofibrous Mats for Antibacterial Application. *Carbohydr. Polym.* **2015**, *117*, 687–693.
- (39) Zhou, B.; Li, Y.; Deng, H.; Hu, Y.; Li, B. Antibacterial Multilayer Films Fabricated by Layer-by-Layer Immobilizing Lysozyme and Gold Nanoparticles on Nanofibers. *Colloids Surfaces & Biointerfaces* **2014**, *116*, 432–438.
- (40) Wang, X.; Cao, W.; Xiang, Q.; Jin, F.; Peng, X.; Li, Q.; Jiang, M.; Hu, B.; Xing, X. Silver Nanoparticle and Lysozyme/tannic Acid Layer-by-Layer Assembly Antimicrobial Multilayer on Magnetic Nanoparticle by an Eco-Friendly Route. *Mater. Sci. Eng. C. Mater. Biol. Appl.* **2017**, *76*, 886–896.
- (41) “What is RNA?” The RNA Society. *RNA*. <https://www.rnasociety.org/about/what-is-rna/>
- (42) “RNA (Ribonucleic Acid).” *The Talking Glossary of Genetic Terms*. National Human Genome Research Institute. <https://www.genome.gov/glossary/index.cfm?id=180>.
- (43) Houseley, J.; Tollervey, D. The Many Pathways of RNA Degradation. *Cell* **2009**, *136*, 763-776.
- (44) Tripathy, D. R.; Dinda, A. K.; Dasgupta, S. A Simple Assay for the Ribonuclease Activity of Ribonucleases in the Presence of Ethidium Bromide. *Analytical Biochemistry* **2013**, *437*, 126-129.
- (45) Millar, D. P.; Robbins, R. J.; Zewail, A. H. Direct Observation of the Torsional Dynamics of DNA and RNA by Picosecond Spectroscopy. *Proc. Natl. Acad. Sci.* **1980**, *77* (10), 5593-5597.

- (46) Chib, R.; Raut, S.; Sabnis, S.; Singhal, P.; Gryczynski, Z.; Gryczynski, I. Associated Anisotropy Decays of Ethidium Bromide Interacting with DNA. *Methods Appl. Fluoresc.* **2014**, *2*, 1-6.
- (47) Kim, H.; Park, Y.; Lee, J. B. Self-assembled Messenger RNA Nanoparticles (mRNA-NPs) for Efficient Gene Expression. *Scientific Reports* **2015**, *5* (12737), 1-9.
- (48) "Polyelectrolytes and Measuring Their Zeta Potential." *Horiba Scientific*. Azo Materials **2018**. <https://www.azom.com/article.aspx?ArticleID=16097>.
- (49) Zhu, R.; Song, J.; Ma, Q.; Zhou, Y.; Yang, J.; Shuang, S.; Dong, C. A Colorimetric Probe for the Detection of Aluminium Ions Based on 11-Mercaptoundecanoic Acid Functionalized Gold Nanoparticles. *Anal. Methods* **2016**, *8*, 7232-7236.
- (50) Routh, P.; Garai, A.; Nandi, A. K. Optical and Electronic Properties of Polyaniline Sulfonic Acid-Ribonucleic Acid-Gold Nanobiocomposites. *Phys. Chem. Chem. Phys.* **2011**, *13*, 13670-13682.
- (51) "Ostwald Ripening." Particle Sizing Systems. *Entegris* **2018**. <http://pssnicomp.com/definitions/ostwald-ripening/>
- (52) Hansen, C. Ostwald Ripening. *Soft-Matter* **2008**.
- (53) Ingham, B.; Lim, T. H.; Dotzler, C. J.; Henning, A.; Toney, M. F.; Tilley, R. D. How Nanoparticles Coalesce: An in Situ Study of Au Nanoparticle Aggregation and Grain Growth. *Chem. Mater.* **2011**, *23*, 3312-3317.
- (54) Jahanshahi, M.; Babaei, Z. Protein Nanoparticle: A Unique System as Drug Delivery Vehicles. *African Journal of Biotechnology* **2008**, *7* (25), 4926-4934.
- (55) Panyam, J. Solid-State Solubility Influences Encapsulation and Release of Hydrophobic Drugs from PLGA/PLA Nanoparticles. *Journal of Pharmaceutical Sciences* **2004**, *93* (7), 1804-1814.
- (56) Snedeker, L. P.; Risbud, A. S.; Masala, O.; Zhang, J. P.; Seshadri, R. Organic Phase Conversion of Bulk (Wurtzite) ZnO to Nanophase (Wurtzite and Zinc Blende) ZnO. *Solid State Sciences* **2005**, *7* (12), 1500-1505.